Burial and temperature evolution in thrust belt systems: Sedimentary and thrust sheet loading in the SE Candian Cordillera

Hardebol, N.J.; Callot, J.P.; Bertotti, G.V.; Faure, J.L.

published in
Tectonics
2009

DOI (link to publisher)
10.1029/2008TC002335

document version
Publisher's PDF, also known as Version of record

Burial and temperature evolution in thrust belt systems: Sedimentary and thrust sheet loading in the SE Canadian Cordillera

N. J. Hardebol,[1,2] J. P. Callot,[1] G. Bertotti,[2] and J. L. Faure[1]

Received 12 June 2008; revised 31 December 2008; accepted 17 February 2009; published 23 May 2009.

[1] The southern Canadian foreland fold-and-thrust belt (FFTB) (SW Alberta–SE British Columbia) records the interplay between foreland basin evolution with the deforming wedge and thus controls the regional-scale overburden and exhumation history. Overburden estimates are typically based on the assumption that peak burials were reached by sedimentary burial prior to the emplacement of thrust sheets. This study combines organic maturity ranks from a newly compiled catalog with forward thermokinematic modeling to examine this assumption. The organic maturity rank trends correlate not only to sedimentary but also to tectonic burial histories. The forward thermokinematic modeling builds on this combined burial history scenario and shows how required peak burial and temperatures can be achieved with reduced sedimentary overburden when combined with tectonic loading. We thus consider that the overburden was reached during instead of prior to the contraction of the FFTB as result of an integrated sedimentary and tectonic burial history. Thermokinematic modeling also suggests that first-order steady state temperature conditions prevail during the development of the FFTB. Differently from earlier findings that considered a drop in paleotemperature gradient during the belts growth, steady state conditions reduce the amount of regional overburden required and, consequently, of eroded sediments. Besides tracing the regional evolution, organic maturity ranks are also affected by more local phenomena such as thrust-scale denudation patterns and fluid flow. **Citation:** Hardebol, N. J., J. P. Callot, G. Bertotti, and J. L. Faure (2009), Burial and temperature evolution in thrust belt systems: Sedimentary and thrust sheet loading in the SE Canadian Cordillera, *Tectonics*, *28*, TC3003, doi:10.1029/2008TC002335.

1. Introduction

[2] Paleotemperature and burial exhumation history estimates are inherently integrated when they are deduced from paleotemperature proxies as burial and exhumation magnitudes depend strongly on the paleogeothermal field, which evolves temporally during orogenesis. The conversion of paleotemperature proxies into burial and erosion estimates requires a careful assessment of the forward kinematic (i.e., deformation, burial, and exhumation) and concurrent paleotemperature histories.

[3] In foreland fold-and-thrust belt (FFTB) systems, burial and exhumation occur under influence of foredeep flexure and deposition combined with thrust sheet emplacement and erosion. Burial can result from a combination of sedimentary loading in the foredeep and subsequent stacking from overriding thrust sheets. Evaluation of burial and exhumation histories from thrust belt systems require an integrated approach in which the response of paleotemperature proxies to combined sedimentary and tectonic loads is tested, e.g., by forward thermokinematic modeling [e.g., *Deville and Sassi*, 2006; *Sassi et al.*, 2007].

[4] Forward thermokinematic modeling integrates burial and exhumation histories and predicts temperature evolution [e.g., *Batt and Brandon*, 2002; *Ehlers and Farley*, 2003]. As end-members, temperature fluctuations either record a combined vertical motion and denudation history relative to a stationary thermal field, or reflect thermal perturbations relative to a fixed material frame resulting from for instance changes in basal heat flow or sedimentary blanketing effects. Several studies have examined the possibility of heat advection for thrust belt systems; from fault block motions [e.g., *Brewer*, 1981; *Husson and Moretti*, 2002; *ter Voorde et al.*, 2004; *Sassi et al.*, 2007] or from fluid flow [e.g., *Forster and Smith*, 1989; *Bodri and Rybach*, 1998].

[5] The southern Canadian foreland fold-and-thrust belt (SW Alberta–SE British Columbia) provides an ideal site for studying the interdependency of the thermal and kinematic evolution of thrust belt systems because of abundant organic maturity measurements and a well-constrained structural evolution. Numerous studies have discussed the burial and thermal history and implications for organic maturation in the FFTB [e.g., *Hacquebard and Donaldson*, 1974; *Pearson and Grieve*, 1985; *Langenberg and Kalkreuth*, 1991; *Osadetz et al.*, 1992; *Langenberg et al.*, 1998]. Furthermore, ample structural work has been performed since *Bally et al.* [1966] provided the first balanced cross sections through the region delineating thin-skinned contractional tectonics [*Dahlstrom*, 1970, *Price*, 1981; *Price and Fermor*, 1985; *Fermor and Moffat*, 1992].

[6] This study pursues a combined analytical and modeling approach to achieve better constrained overburden estimates through time. It builds on existing and new pale-

[1]Institut Français du Pétrole, Rueil Malmaison, France.
[2]Netherlands Research Centre for Integrated Solid Earth Sciences, Faculty of Earth and Life Science, Vrije Universiteit, Amsterdam, Netherlands.

0278-7407/09/2008TC002335$12.00

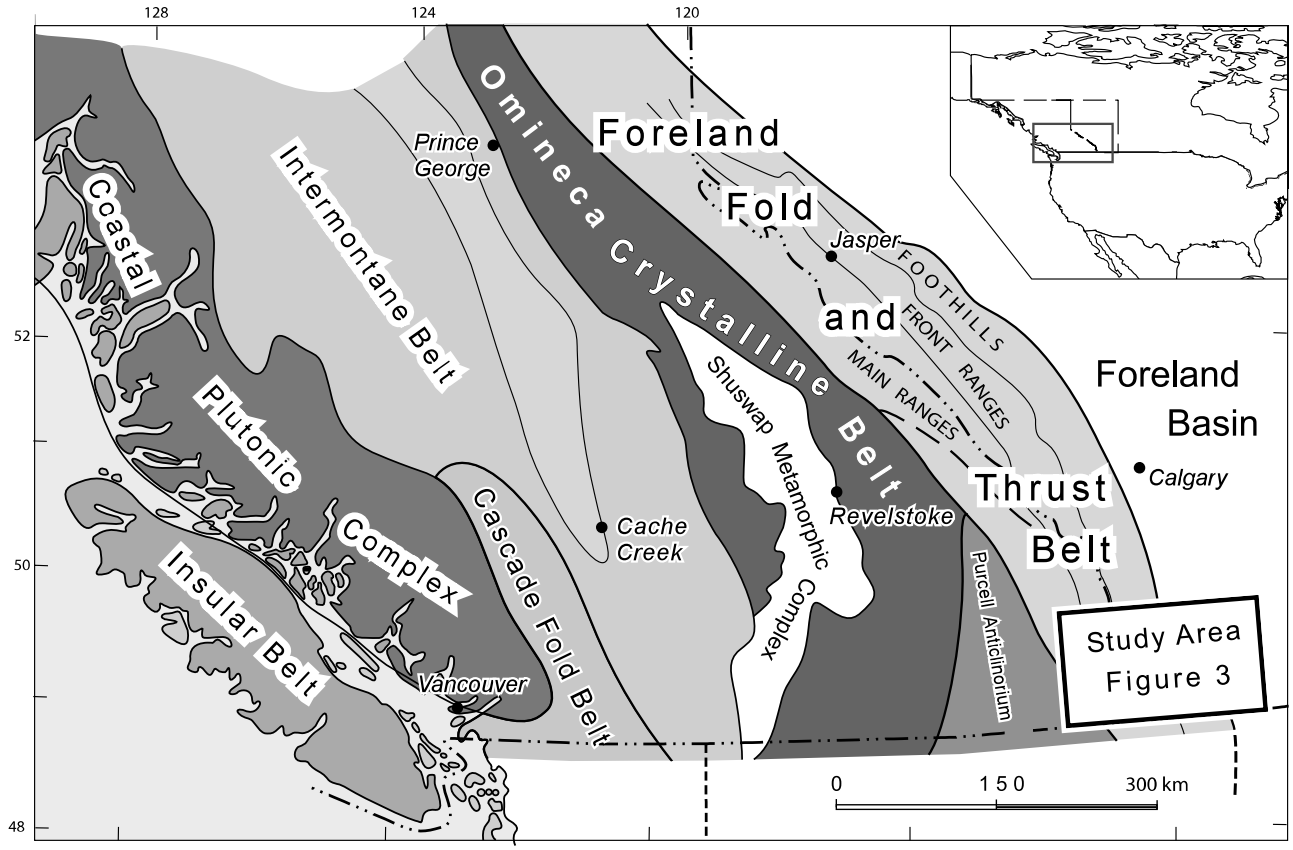

Figure 1. Overview map of the southern Canadian Cordillera outlining its morphotectonic subdivision and location of the study area.

otemperature proxies combined with 1-D and 2-D kinematic modeling studies to enhance burial exhumation history predictions of the structurally complex FFTB system [*Faure et al.*, 2004; *Osadetz et al.*, 2004; *Roure et al.*, 2005; *Hardebol et al.*, 2007]. We aim at discerning between the sedimentary and tectonic burial components to determine the amounts of sediments that once buried the belt and has subsequently been removed. In particular, we challenge the widespread notion that peak temperatures were reached during purely sedimentary burial [e.g., *Hacquebard and Donaldson*, 1974; *Hacquebard*, 1977]. We will first examine organic maturity rank trends from a newly compiled data set that yields a dense regional coverage for the southeastern Canadian FFTB. The catalog contains vitrinite reflectance (VR) and Tmax measurements from Rock-Eval pyrolyses, from both literature and newly acquired surface and borehole samples. By plotting data onto maps, stratigraphic columns and structural cross sections, we evaluate the burial exhumation history by distinguishing between the sedimentary and tectonic overburden components and inferring the paleogeothermal evolution.

[7] This paper continues with a more detailed description of the interplay between a progressively deforming FFTB and temperature and organic maturation histories. Second, this study explores the chance for spatial and temporal variations in paleogeothermal field during the evolution of the thrust belt system and how this affects regional-scale overburden predictions. Forward thermokinematic models test the significance of heat advection from fault block motions for a specified deformation history of the study area. The modeling is performed for detailed structural cross sections that provide thermal and organic maturation history predictions that permit comparison with our organic maturity ranks.

2. Geologic Context

2.1. Regional Geologic Context

[8] The southern Canadian foreland fold-and-thrust belt (FFTB) bounds the eastern edge of the Canadian Cordillera (Figure 1). This northeastward tapering contractional wedge is a result of the Late Cretaceous–Paleocene orogeny along the North American margin [*Gabrielse and Yorath*, 1992]. The belt is bounded to the west by the Rocky Mountain Trench and to the east by the undeformed foreland basin (Figure 2a). The study area comprises a strongly shortened series of Mesoproterozic, Paleozoic and Mesozoic strata scraped off in a series of thrust sheets and emplaced over the underlying North American craton [*Price*, 1981; *Price and Fermor*, 1994]. The Mesoproterozic Belt–Purcell Supergroup (Figure 2b) consists of an up to 10 km thick shallow

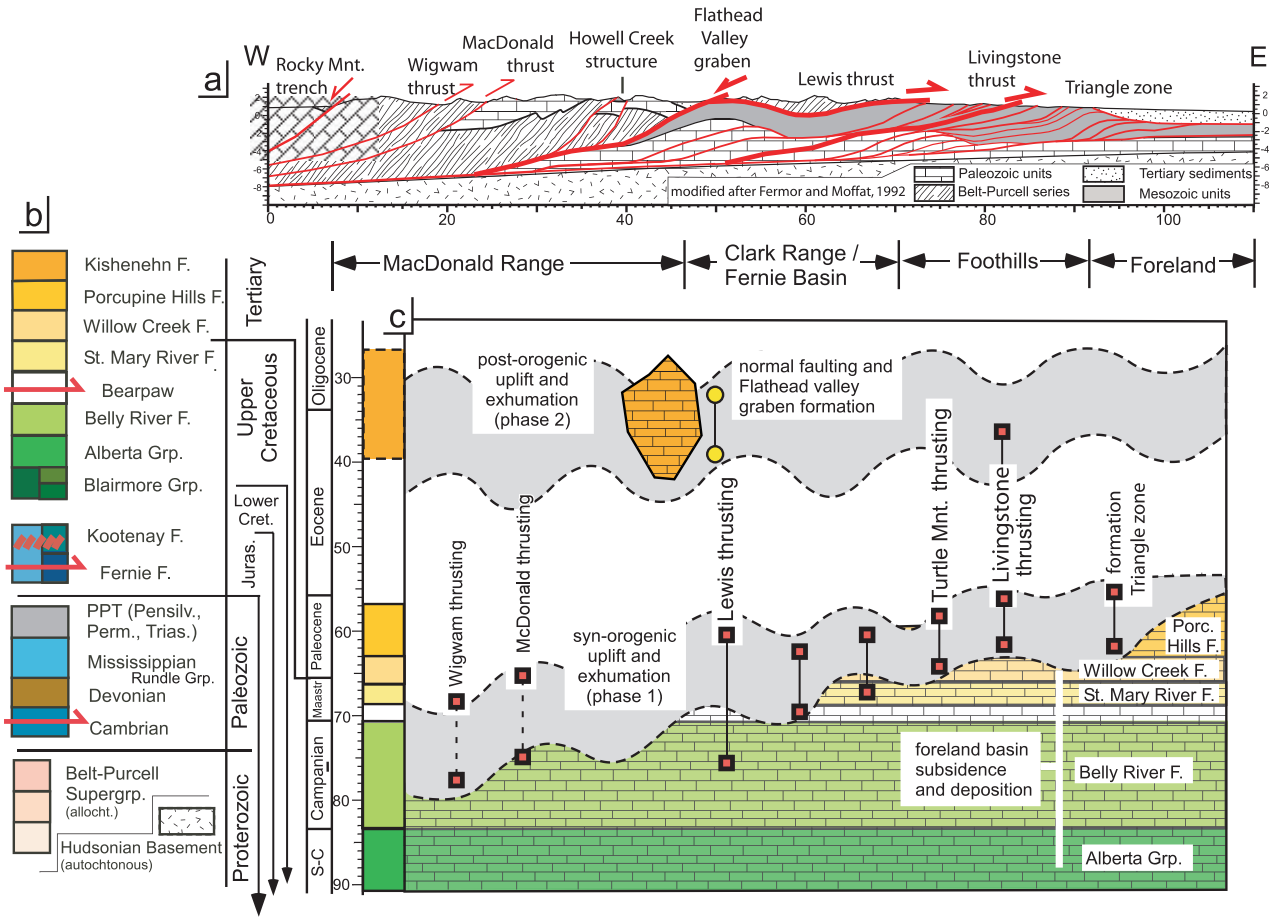

Figure 2. Overview chart of the geologic context of the study area. (a) Structural cross section (simplified after *Fermor and Moffat* [1992]) denoting the main structural features, including the Rocky Mountain trench in the west and the eastward Lewis thrust, the Livingstone thrust, and triangle zone. Further note how the Paleozoic series are stacked into two duplex systems, detached from overlying Mesozoic series at the Fernie shales. Cross section location is shown in Figure 3 marked as profile C. For further details, see *Hardebol et al.* [2007]. (b) Lithostratigraphic subdivision with a change between the Paleozic to Mesozoic series from passive margin into foredeep deposition. The Eo-Oligocene Kishenehn Formation is deposited in an extensional graben system and marks overall cessation of contraction in the belt. (c) Time chart of Upper Cretaceous (Santonian-Campanian) to Paleogene (Oligocene) deformation history outlining temporal relationship between the main events (i.e., subsidence and deposition, faulting sequence, uplift and exhumation). This forward deformation sequence is also followed in our kinematic modeling, and more details are given by *Hardebol et al.* [2007]. Contractional deformation started post-80 Ma farther to west, constrained by the dating of decollement level to polydeformed sillimanite-orthoclase paragneisses [*Parrish*, 1995; *Carr*, 1992], and overall shortening ceased at ~58 Ma [*Fermor and Moffat*, 1992; *Sears*, 2001; *van der Pluijm et al.*, 2006]. Cooling curves suggest rapid uplift and erosion of the Purcell Anticlinorium (just west of the study area) between 65 and 55 Ma [*Archibald et al.*, 1984] and FT T-t modeling for Lewis thrust hanging wall cooling 110–60°C between 75 and 35 Ma.

water limestones and siliciclastic infill of an intracontinental basin [*Price and Sears*, 2000]. The overlying Paleozoic consists of a predominately carbonate platform-to-basin succession. The change to the Mesozoic clastics marks the onset of the foreland basin development under influence of an orogen encroaching from the west. Mesozoic clastics dominate the frontal "foothills" region. The sequence contains several organic rich layers including the Kootenay Group that comprises several coal seams, and an organic rich marine shale interval at the base of the Alberta Group (i.e., Blackstone Formation). The Cretaceous Belly River Formation comprises a thick synorogenic sequence, important for evaluating restored sedimentary thicknesses and timing of thrust fault activation. Paleocene units are absent in the belt, but found in the proximal undeformed foreland basin close to the FFTB front. Here, a thin remnant of a supposedly much thicker original sequence is found, while the topmost part of the Paleocene sequence (i.e., the Porcupine Hills Formation;

Figure 2b) is only present at further distance from the belt. The lithostratigraphic succession of the foreland belt ends with localized deposits of the Eo-Oligocene Kishenehn Formation as basin infill of the Flathead valley half graben system (Figure 2a).

2.2. Main Structures and Kinematics

2.2.1. The Lewis Thrust Sheet

[9] The Lewis thrust sheet (LTS) is the longest thrust sheet of the FFTB and its displacement accounts for half of the total shortening accommodated in the southern part of the belt [*Fermor and Moffat*, 1992; *Price and Fermor*, 1994]. Its kinematics and structural style are strongly controlled by along-strike changes in the basal decollement geometry inherited from the Mesoproterozoic and lower Paleozoic basin architecture [*Price and Sears*, 2000]. In the Clark Range (Figures 2a and 3), the LTS is represented by a thin erosional remnant of a formerly much thicker Mesoproterozoic to Mesozoic sedimentary succession (Figure 2) [*Osadetz et al.*, 2004]. Northward, the Lewis thrust basal decollement forms a lateral ramp that follows the pinch-out of the Mesoproterozoic basin fill and uses a shallower decollement level in the lower Cambrian strata. While the LTS is deeply denudated to Mesoproterozoic level in the Clark Range, Mesozoic strata are still preserved in the Fernie Basin syncline (Figure 3) where the basal decollement is positioned at shallower stratigraphic levels (Figure 4). The preservation of various coal seams in the Jurassic Kootenay Formation of the Fernie Basin provides a rich source for organic maturity rank sampling.

[10] The ~100 km eastward translation of the LTS over a major flat and ramp system that cuts through the Paleozoic and Mesozoic series, emplaces Mesoproterozoic units onto Cretaceous Belly River sediments. Sediments in the LT footwall supported by dating of fault gouge [*van der Pluijm et al.*, 2006] indicate thrusting probably continued till the earliest Paleocene (58 Ma; see Figure 2c).

2.2.2. The Foothills

[11] The area east of the Lewis thrust front (Figure 2a) forms the footwall of the Lewis thrust sheet and is referred to as the ''foothills.'' The foothills area is characterized by closely spaced easterly verging imbricate thrust slices that contain Mesozoic to Cenozoic clastics deposited in front of the deforming wedge (Figures 2 and 3). The clastics overly Paleozoic carbonates and are decoupled along the Fernie shales that serves as a major decollement interval. The Paleozoic are detached from the undeformed basement by widely spaced thrust sheets that form large antiformal stacks (Figure 3). The Turtle Mountain and Livingstone thrusts (Figure 3) are the dominant thrusts east of the Lewis thrust and are part of antiformal stacks in the Paleozoic series. The Lewis thrust sheet is folded by the duplex systems, what requires that displacement of the foothills thrust sheets postdate LT displacement (Figure 2c). In general, the timing of the activities of the thrusts is poorly conditioned. Direct dating of thrust sheet activity, such as available for the LT, is not commonplace and the timing foothills thrust sheet motions lack direct time constraints. They have presumably followed in-sequence activation from west to east [e.g., *Price*, 1981, 2001; *Price and Fermor*, 1985].

[12] Paleozoic carbonates carried by the Livingstone thrust override Late Cretaceous foredeep clastics. This forms an exception to the prevalent structural style of the foothills where the allochtonous Paleozoic units stay decoupled from and are covered by thrust sheet imbricates of Mesozoic series (Figure 4). The Turtle mountain duplex system illustrates this contrast well by exposing Mississippian carbonates atop of Belly River strata, thus carried by a Livingstone thrust that cuts through the Fernie shale decollement interval (see Figures 2a and 2b for general outline and Figure 4 for detailed cross sections). To the east, the foothills are bordered by a back thrust which uses the late Campanian Bearpaw shales as decollement level. The overlying Maastrichtian and Paleocene clastics, decoupled from the underlying imbricated Mesozoic units of the triangle zone, are not strongly deformed but show a gentle eastward tilt. The main contraction in the foothills presumably occurred in Paleocene times with concurring sedimentation of St. Mary River to Porcupine Hills formations in the foredeep (Figure 2c).

2.2.3. Eo-Oligocene Half Grabens

[13] The FFTB shows also evidence of normal faulting commonly reactivating older contractional features. In the study area, the Flathead normal fault is a listric normal fault that uses the Lewis thrust as decollement level. It dissects the LTS with up to 12 km of downward motion, forming the eastern border fault of the late Oligocene Flathead half graben (Figures 2 and 3) [*Bally et al.*, 1966; *McMechan and Price*, 1980; *Fermor and Moffat*, 1992; *Constenius*, 1996].

[14] The Flathead normal fault and graben are important features to constrain original overburdens and timing of the exhumation of the FFTB. The MacDonald Range, located west of the Flathead normal fault, forms the down-faulted block relative to the Clark Range as hanging wall east of the fault (Figure 2). The down throw of the MacDonald Range has lead to good preservation of the Paleozoic and Mesozoic strata. As a result, a small patch of the Late Cretaceous Wapiabi Formation (i.e., upper Alberta Group) is well preserved in the Howell Creek structure that forms a small further down-faulted sliver of this hanging wall. The Howell Creek structure thus presents the westernmost direct proof of a former more widespread Late Cretaceous overburden to the belt. In addition, erosional products from Blairmore strata are found in the Eo-Oligocene basin fill of the Flathead valley graben. Assuming the Clark Range as its most likely source, this suggests that a 5–6 km thick Lewis thrust sheet inclusive of the Blairmore Formation, remained preserved from erosion till the formation of the Flathead valley graben in Eo-Oligocene times [*Sears*, 2001; *Osadetz et al.*, 2004].

2.3. Previous Work on Overburden and Paleogeothermal Estimates

[15] Numerous burial history and paleogeothermal studies have been performed in the past and provide overburden estimates for the undeformed foreland basin and FFTB.

[16] In a foreland basin, burial evidently occurs by sedimentary loading and simple assumptions on concurring thermal

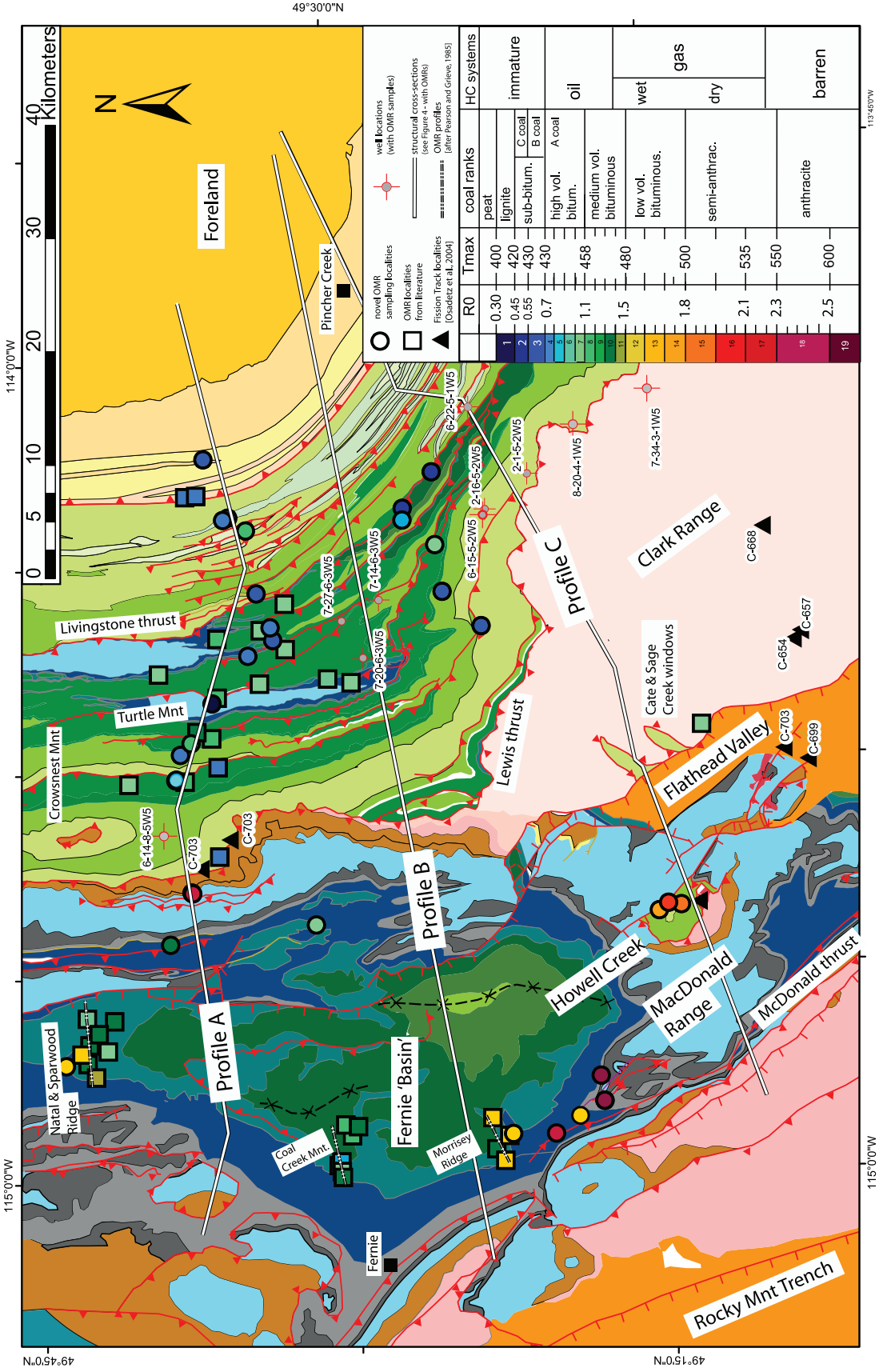
49°30'0"N
114°0'0"W
115°0'0"W
113°45'0"W
49°45'0"N
49°15'0"N
0 5 10 20 30 40 Kilometers
N
Foreland
Pincher Creek
Livingstone thrust
Turtle Mnt
Crowsnest Mnt
Natal & Sparwood Ridge
Coal Creek Mnt
Morrisey Ridge
Fernie
Fernie 'Basin'
Profile A
Profile B
Profile C
Lewis thrust
Howell Creek
MacDonald Range
McDonald thrust
Clark Range
Cate & Sage Creek windows
Flathead Valley
Rocky Mnt Trench
6-14-8-5W5
C-703
7-27-6-3W5
7-14-6-3W5
7-20-6-3W5
6-15-5-2W5
2-16-5-2W5
6-22-5-1W5
2-1-5-2W5
8-20-4-1W5
7-34-3-1W5
C-668
C-657
C-654
C-699
well locations (with OMR samples)
structural cross-sections (see Figure 4 - with OMRs)
OMR profiles [after Pearson and Grieve, 1985]
novel OMR sampling localities
OMR localities from literature
Fission Track localities [Osadetz et al., 2004]
R0
Tmax
coal ranks
HC systems
peat
lignite
sub-bitum.
high vol. bitum.
medium vol. bituminous
low vol. bituminous.
semi-anthrac.
anthracite
C coal
B coal
A coal
immature
oil
gas
wet
dry
barren

Figure 3

histories are deduced which can allow for a relatively simple translation of organic maturity ranks to overburden estimates. At present, only a thin veneer of the Paleocene Porcupine Hills formation is preserved in the proximal basin close to the deformation front. A significant additional sedimentary load of 2–5 km thickness is required atop of the present-day Cretaceous to Paleocene basin fill to explain the observed organic maturity ranks [e.g., *Hacquebard*, 1977; *England and Bustin*, 1986b; *Kalkreuth and McMechan*, 1988; *Osadetz et al.*, 1992; *Bustin*, 1991]. Unaffected by the Laramide orogeny, the exhumation in the basin presumably occurred in Eo-Oligocene times (Figure 2c).

[17] Also for the deformed belt, studies have examined the overburden and exhumation history [e.g., *Hacquebard and Donaldson*, 1974; *Pearson and Grieve*, 1985; *Langenberg and Kalkreuth*, 1991; *Langenberg et al.*, 1998]. Like for the basin, some studies considered that organic maturity ranks in the belt result from peak temperatures from preorogenic sedimentary burial, whereas others have pointed to the effect from thrust sheet loading [*Hacquebard and Donaldson*, 1974; *Hacquebard*, 1977; *England and Bustin*, 1986a]. More recently, fission track [*Osadetz et al.*, 2004] and thermokinematic modeling studies [*Faure et al.*, 2004; *Hardebol et al.*, 2007] strengthen renewed burial history appraisal for these structurally complex areas.

[18] Furthermore, various studies have produced paleotemperature gradient estimates for the study area for Late Cretaceous to Tertiary times [*Currie and Nwachukwu*, 1974; *Hitchon*, 1984; *McMechan and Price*, 1982; *Middleton*, 1982]. The studies entail quite some spread in estimated gradients, partly inherited from spatial and temporal paleogeothermal variations, but also as result of different overburden assumptions. *Osadetz et al.* [1992] summarizes these findings with a regional-scale assessment of thermicity in foothills and proximal basin areas during and after the Laramide deformation history and provides paleogeothermal gradient estimates in the order of 22–28°C km^{-1}.

[19] Fluctuations in the paleotemperature gradient have been proposed. *Osadetz et al.* [2004] infers a paleotemperature gradient of ~10°C km^{-1} for the 75 to 60 Ma time interval from AFT t-T modeling of samples from Belt Purcell rocks at the base of the LT hanging wall in the Clark Range. This would give a rough indication of the paleogeothermal gradient inferred over a stratigraphic interval of 638 m and might suggest depressed paleogeothermal gradients during thrusting of the Lewis thrust sheet [*Osadetz et al.*, 2004; *Cooley et al.*, 2006]. A temperature gradient of ~20–25°C km^{-1} was considered to represent the ambient background geotherm under steady state conditions prior to motion. Also, *Hitchon* [1984] appeals to a change in paleotemperature field of the foothills and proximal basin for mid-Eocene time as result of changes in the geomorphology and hydrodynamic system.

3. Temperature and Burial History Estimates From Organic Maturity Ranks

3.1. Introduction

[20] Organic maturity rank (OMR) data provide information on temperature and, indirectly, on burial histories [e.g., *Teichmüller*, 1986; *Tissot et al.*, 1987]. OMR data are often interpreted to result from peak temperatures acquired at the time of maximum sedimentary burial. However, the OMRs do not simply record the peak temperature, as the finite maturation rank results from a composite effect of time and temperature [*Sweeney and Burnham*, 1990; *Tissot*, 2003]. Differently from fission tracks (FT), they do not allow for modeling t-T pathways but their abundance in regional-scale overburden studies make them a helpful tool.

[21] This study uses two types of OMRs. The first, vitrinite reflectance (VR) is an optic measure of the reflectivity of the organic maceral (terrestrial plant tissue referred to as kerogen type III) and uses it as proxy of its thermal maturation [e.g., *Tissot et al.*, 1987]. Tmax, on the other hand, is a maturation indicator obtained from Rock-Eval pyrolyses and defined by the pyrolyses temperature at which a maximum amount of hydrocarbon compounds is being released from the kerogen [*Espitalié*, 1986] and can be used for both type II and type III kerogens. Rock-Eval pyrolysis method is a specific kerogen evaluation procedure used to identify the type and maturity (Tmax) of organic matter by a programmed temperature heating and cracking of organic matter in a rock sample [*Espitalié*, 1986].

[22] We have built a catalog of paleotemperature proxies that contains OMRs from new surface samples and well cuttings and are combined with OMRs from literature (Table 1). They cover a total of more than 200 localities, many data points representing in reality averages from several samples. A variety of attributes are stored in the catalog, including OMR type (i.e., VR or Tmax from Rock-Eval pyrolyses), stratigraphic and geographic position, and in case of pyrolyses data, also total organic carbon contents (TOC) and, oxygen and hydrogen indices (i.e., OI and HI) as kerogen-type indicator. Furthermore, the examination of our OMR data set includes the distinction of kerogen types from the

Figure 3. Structural map of the study area including the position of structural cross sections (Figure 4) and of OMR sample and well locations and fission track sampling locations after *Osadetz et al.* [2004]. The map depicts an extensive set of OMR data that contain a novel set of Tmax values from Rock-Eval pyrolyses [*Peters*, 1986] from surface samples and well cuttings. Furthermore, a dense set of maturity ranks from literature is included: from *Hacquebard and Donaldson* [1974] with samples from the foothills and Crowsnest Pass area and from *Pearson and Grieve* [1985] from across the Fernie Basin. Furthermore, maturity ranks from several wells and surface samples for the foreland and foothills areas have been taken from Geological Survey of Canada open file reports [*Snowdon*, 1997; *Stasiuk and Fowler*, 2002] and several other wells (i.e., 7-34-3-1W5 and 6-14-8-5W5) and a few surface samples from a variety of reports [*Cooley et al.*, 2006; *Hannigan et al.*, 1993; *Langenberg et al.*, 2002]. The legend gives a correlation table between Ro and Tmax, petroleum systems, and a color table utilized for our OMR categorization.

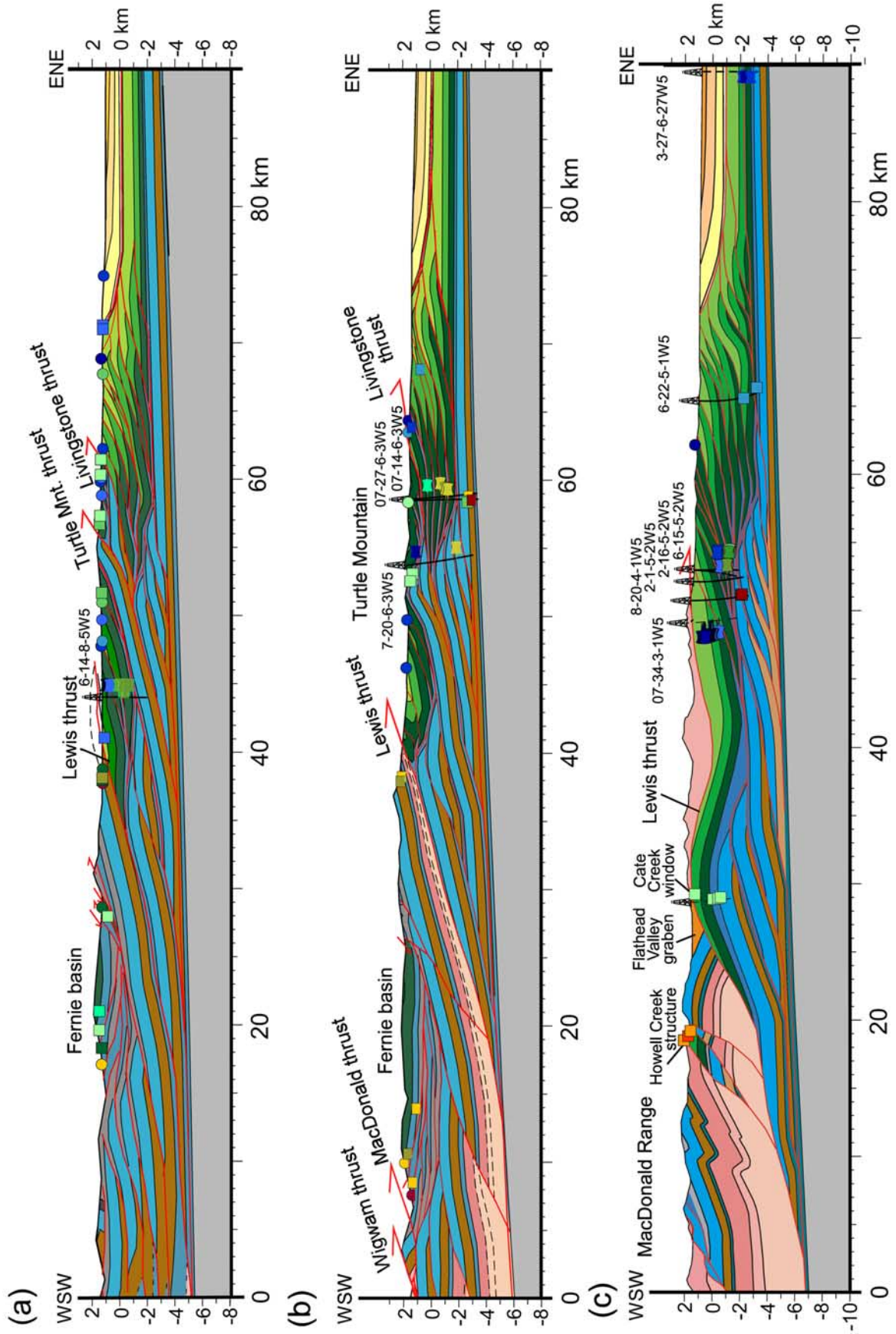

Figure 4. Structural cross sections with organic maturity ranks plotted to their structural position (see Figure 3 for their locations). The lithostratigraphic subdivision follows Figure 2b. For the OMR categorization, see the legend of Figure 3.

provided oxygen and hydrogen indices of the Tmax data that precise correlation to corresponding VR values [e.g., *Espitalié*, 1986; *Durand et al.*, 1986; *Tissot*, 2003].

[23] The OMR data is first presented in map view showing the rank distribution at the surface (Figure 3). A correlation chart between Tmax temperature and VR rank values, along with a OMR category subdivision is given in Figure 3 as well. This chart (Figure 3) depicts the beginning of the oil zone at a VR value of 0.5%Ro and corresponding Tmax value of 430°C [e.g., *Espitalié*, 1986; *Teichmüller*, 1986].

[24] Figure 3 also gives the location of well sites for which this study presents various new OMRs from core cuttings. Last, the positions of the structural cross sections (Figure 4) are shown [see also *Hardebol et al.*, 2007]. We have plotted the OMR distribution from subsurface samples on these cross sections.

[25] At first order, the present-day erosion front of the Lewis thrust separates an area to the west with overall higher values from one to the east with lower values. West of the Lewis thrust front, maturity ranks are generally higher with VR values ranging between 1.1 to 1.6%Ro and with values of ~1.3%Ro dominating. East of the Lewis thrust front, in the foothills, OMR ranks are about 0.6–0.7%Ro with higher values to 1.2–1.3%Ro. High values from the Lewis thrust sheet are apparent in samples across the Fernie Basin, where ranks of 1.2–1.4%Ro (and corresponding Tmax of 460–475°C) are common [e.g., *Pearson and Grieve*, 1985].

3.2. OMR Distribution and Sedimentary Burial

[26] To explore correlations between OMRs and stratigraphic depth, we have plotted the rank values from two wells (Figure 5) both located in the footwall of the Lewis thrust. Well 6-14-8-5W5 is located just east of the present-day Lewis thrust erosion front, whereas well 7-34-3-1W5, located in the Clark Range, is covered by a thin erosional remnant of a previously much thicker LTS (see Figures 3 and 4 for their location and structural context). Both wells comprise a succession of Cretaceous Alberta and Blairmore Group underlain by the Jurassic Kootenay and Fernie Formations (see Figure 2b for the stratigraphy).

[27] OMRs plotted against stratigraphic depths would show rank increase with depth when sedimentary burial had governed the maturation history. On the whole, the OMRs in the wells show a wide scattering and exhibit a poor correlation with stratigraphic depth. The best correlation is shown in the uppermost thrust unit of well 7-34-3-1W5. For the underlying thrust sheet of well 7-34-3-1W5 and for the thrust units of well 6-14-8-5W5 (Figure 5a), no meaningful regression line can be drawn. Only indicative ellipses are plotted that outline a sedimentary burial trend. Overall however, correlation with stratigraphic depth as indication of sedimentary burial is poor for these individual wells.

[28] We have also plotted the complete OMR data set against their stratigraphic position (Figure 6). The vertical position of the sample is obtained considering a restored stratigraphic depth of the sample by choosing regional averaged thicknesses for the different lithostratigraphic units. Samples are grouped for individual wells (diamonds) and structural entities (circles for Fernie Basin and triangles for foothills) and comprise a dense coverage for the Kootenay coal intervals and the lowermost Blairmore Group. On the whole, there is a general trend of increasing OMRs to stratigraphic depth. The ellipses show the perceived correlation to stratigraphic depth. On the other hand, a large amount of OMRs give such a wide scatter in rank values from corresponding Fernie coals and lowermost Blairmore units across different structural entities. Therefore, a consistent stratigraphic burial trend is disregarded. Together with the above discussed OMR distribution from two wells, it shows the difficulty to explain the observed OMR distribution in the FFTB mainly by sedimentary burial.

3.3. Signatures of Tectonic Overburden

[29] The effect of the structural position on the distribution of maturity ranks is further examined plotting the OMRs on the structural cross sections (Figure 4). The profiles give some of the surface samples that are located in proximity of the transects and particularly depict the OMR samples from our data set that are derived from well cuttings. A collection of wells (i.e., wells 8-20-4-1W5, 2-1-5-2W5, 2-16-5-2W5, 6-15-5-2W5) that sample the same Blairmore and Kootenay intervals (Figure 4c) exhibit, for the same stratigraphic interval, Tmax values of 440–450°C at 2 km and 470–480°C at 3–3.5 km depth. In addition, another cluster of wells from around the Turtle mountain duplex (i.e., 7-20-6-3W5 penetrating the antiformal stack and 7-14-6-3W5, 7-27-6-3W5 located in front of the stack; Figure 4b) also sample the same intervals at increasing structural depths. They again show increasing Tmax values of ~440–460°C from surface to 1000 m depth and 480–490°C at 3000 m. OMR distributions would be indifferent to the structural position samples hold only when the deformation had no significant effect on the maturation history. However, these samples give increasing Tmax values for the same stratigraphic unit at greater structural burial depths.

[30] The effect of structural position on the rank distribution may also be shown in the detailed plots of the earlier introduced two wells (Figure 5). Well 6-14-8-5W5 (Figure 5a) includes one duplication of the upper Blairmore Group, whereas 7-34-3-1W5 (Figure 5b) exhibits a fourfold repetition of the Blairmore to Fernie succession. The OMRs from the Blairmore Group of the basal unit in well 6-14-8-5W5 exhibit comparable values as the overlying yet stratigraphic lower Kootenay Formation. This is also shown in Figure 6, where the well samples of 6-14-8-5W5 from the upper Blairmore yield higher values than the stratigraphic lower Kootenay samples as they come from a structural lower unit. The lower portion of well 7-34-3-1W5 comprises such a strong imbrication that both stratigraphic and structural trend are difficult to discern.

[31] Furthermore, when the OMRs between the two wells are compared from the same stratigraphic levels, well 6-14-8-5W6 shows discernable higher Tmax values of 470–480°C against 450–455°C for well 7-34-3-1W5. This again shows that the OMR ranks do not simply correlate to their stratigraphic position between different structural entities. The structural position affects OMR values and thus not only

Table 1. Slice Through Our Newly Compiled OMR Catalog, Giving an OMR and Lithological Description of the Samples

			OMR				Lithostratigraphic	
Code	Source[a]	Locality	Type	Rank	Category	VR[b]	Unit[c]	Approximate Depth[d] (m)
1-0	1	Paegan Indian reserve	Tmax	449	4	0.78	PCPL	750
1-5	1	Waterton_Dam_North	Tmax	531	17	2.75	WLCK	2250
1-17	1	well 03-27-006-27W4	Tmax	442	3	0.63	SMRR	3500
3-17	3	distal foothills/location 18	VR	0.8	4	0.76	BLRV	5500
1-15	1	Livingstone thrust unit/Burmis	Tmax	453	6	0.93	BLRV	5500
3-18	3	distal foothills/location 18	VR	0.8	4	0.76	BLRV	5500
1-6	1	Waterton Dam South	Tmax	429	1	0.43	BLRV	5500
1-16	1	Livingstone thrust unit/Burmis	Tmax	460	8	1.18	BLRV	5500
3-4	3	Turtle Mountain Thrust unit/location 17	VR	0.8	4	0.78	BLRV	5500
1-17	1	Livingstone thrust unit/Burmis	Tmax	443	3	0.63	BLRV	5500
4-138	4	well 07-34-003-01W5	Tmax	430	2	0.50	ABGP	7014
4-137	4	well 07-34-003-01W5	Tmax	433	2	0.50	ABGP	7035
4-136	4	well 07-34-003-01W5	Tmax	432	2	0.50	ABGP	7056
4-135	4	well 07-34-003-01W5	Tmax	435	2	0.58	ABGP	7077
1-48	1	Howell Creek	Tmax	522	16	2.55	WPIB	7250
1-24	1	Turtle Mountain thrust unit	Tmax	448	4	0.78	WPIB	7250
1-49	1	Howell Creek	Tmax	513	15	2.35	WPIB	7250
1-47	1	Howell Creek	Tmax	505	14	2.15	WPIB	7250
4-126	4	well 07-34-003-01W5	Tmax	430	2	0.50	ABGP	7264
4-123	4	well 07-34-003-01W5	Tmax	437	2	0.58	ABGP	7327
4-115	4	well 07-34-003-01W5	Tmax	435	2	0.58	ABGP	7494
4-16	1	well 03-27-006-27W4	Tmax	439	2	0.53	SSPK	7525
4-15	1	well 03-27-006-27W4	Tmax	442	3	0.63	BLCK	7575
4-103	4	well 06-14-008-05W5	Tmax	465	9	1.28	BMGP	7656
4-45	4	well 06-14-008-05W5	Tmax	469	10	1.36	BMGP	7657
4-44	4	well 06-14-008-05W5	Tmax	450	5	0.83	BMGP	7667
4-102	4	well 06-14-008-05W5	Tmax	470	11	1.40	BMGP	7749
4-101	4	well 06-14-008-05W5	Tmax	461	8	1.18	BMGP	7842
4-261	4	well 07-34-003-01W5	Tmax	443	3	0.66	BMGP	7904
4-100	4	well 06-14-008-05W5	Tmax	467	10	1.32	BMGP	7934
4-110	4	well 06-14-008-05W5	Tmax	471	11	1.40	BMGP	8023
3-48	5	R0_5141; well 6-22-5-1W5	VR	0.89	5	0.89	MNVL	8075
3-50	5	R0_80; C-160717	VR	0.6	3	0.61	MNVL	8075
1-23	1	Turtle Mountain thrust unit	Tmax	459	8	1.13	BMGP	8075
1-18	1	Livingstone thrust unit/Burmis	Tmax	449	4	0.78	BMGP	8075
3-51	5	R0_8719; C-248078	VR	0.8	5	0.82	MNVL	8075
1-25	1	Turtle Mountain thrust unit/Coleman	Tmax	452	5	0.83	BMGP	8075
1-26	1	Turtle Mountain thrust unit/Coleman	Tmax	440	3	0.58	BMGP	8075
2-13	2	well 06-15-005-02W5	Tmax	460	8	1.18	BMGP	8075
3-46	5	well 5-1-10-4W5; R0_4611	VR	1.22	9	1.22	MNVL	8075
3-51	5	R0_8719; C-248078	VR	0.8	5	0.82	MNVL	8075
3-55	6	well Sage Creek no. 2 616	VR	1.05	7	1.05	BMGP	8075
3-46	5	well 05-01-010-04W5/R0_4611	VR	1.22	9	1.22	MNVL	8075
3-50	5	R0_80; C-160717	VR	0.6	3	0.61	MNVL	8075
4-202	4	well 07-34-003-01W5	Tmax	429	1	0.43	BMGP	8171
4-97	4	well 06-14-008-05W5	Tmax	460	8	1.18	BMGP	8213
4-107	4	well 06-14-008-05W5	Tmax	463	9	1.23	BMGP	8285
4-96	4	well 06-14-008-05W5	Tmax	463	9	1.23	BMGP	8305
4-122	4	well 06-14-008-05W5	Tmax	454	6	0.98	BMGP	8363
4-95	4	well 06-14-008-05W5	Tmax	466	10	1.32	BMGP	8398
4-259	4	well 06-14-008-05W5	Tmax	449	4	0.78	BMGP	8414
4-49	4	well 06-14-008-05W5	Tmax	459	8	1.13	CDMN	8415
4-27	4	well 06-14-008-05W5	Tmax	448	4	0.78	BMGP	8440
4-120	4	well 06-14-008-05W5	Tmax	464	9	1.28	BMGP	8443
4-114	4	well 06-14-008-05W5	Tmax	462	9	1.23	CDMN	8478
4-104	4	well 06-14-008-05W5	Tmax	459	8	1.13	BMGP	8482
4-94	4	well 06-14-008-05W5	Tmax	464	9	1.28	BMGP	8491
4-63	4	well 06-14-008-05W5	Tmax	460	8	1.18	KTNY	8539
4-62	4	well 06-14-008-05W5	Tmax	463	9	1.23	KTNY	8563
3-30	6	Natal Ridge	VR	1.0	6	0.97	MMTN	8575
3-25	6	Coal Creek Mountain	VR	0.90	6	0.90	MMTN	8575
3-26	6	Coal Creek Mountain	VR	0.8	5	0.82	MMTN	8575
3-20	6	Morrissey Ridge	VR	1.4	11	1.38	MMTN	8575
3-29	6	Coal Creek Mountain	VR	1.2	8	1.18	MMTN	8575
3-27	6	Coal Creek Mountain	VR	1.1	8	1.12	MMTN	8595
3-60	1	well 06-14-008-05W5	Tmax	475	11	1.44	KTNY	8610
3-28	6	Coal Creek Mountain	VR	1.4	10	1.35	MMTN	8615

Table 1. (continued)

			OMR				Lithostratigraphic	
Code	Source[a]	Locality	Type	Rank	Category	VR[b]	Unit[c]	Approximate Depth[d] (m)
3-35	6	Sparwood Ridge	VR	1.1	7	1.05	MMTN	8655
4-58	4	well 06-14-008-05W5	Tmax	465	9	1.28	KTNY	8657
3-16	3	Livingstone thrust unit/location 15	VR	1.1	7	1.08	KTNY	8675
3-7	3	Turtle Mountain Thrust unit/location 7	VR	1.1	8	1.12	KTNY	8675
1-76	1		Tmax	456	7	1.08	KTNY	8675
3-8	3	Turtle Mountain Thrust unit/6	VR	1.2	9	1.24	KTNY	8675
3-53	3	Fernie Basin E/location 1 Tm-2	VR	1.0	7	1.03	KTNY	8675
3-53	3	Fernie Basin E./location 1 Tm-1	VR	1.1	7	1.05	KTNY	8675
3-53	3	Fernie Basin E./location 1 Tm-3	VR	1.0	7	1.02	KTNY	8675
3-53	3	Fernie Basin E./location 1 Tm-4	VR	1.1	7	1.06	KTNY	8675
3-54	3	location 2	VR	1.1	7	1.06	KTNY	8675
2-5	2	well 07-27-006-03W5	Tmax	485	12	1.68	KTNY	8675
1-19	1	Livingstone thrust unit/Bellevue	Tmax	445	3	0.68	KTNY	8675
3-56	4	Sage Creek No. 2 well	VR	1.04	7	1.04	MMTN	8675
3-57	4	Sage Creek No. 2 well	VR	1.06	7	1.06	MMTN	8675
2-22	2	well 07-20-006-03W5	Tmax	476	12	1.53	KTNY	8675
2-21	2	well 07-20-006-03W5	Tmax	438	2	0.53	KTNY	8675
1-14	1		Tmax	438	2	0.53	KTNY	8675
2-2	2	well 07-14-006-03W5	Tmax	482	12	1.63	KTNY	8675
2-1	2	well 07-14-006-03W5	Tmax	453	6	0.93	KTNY	8675
3-9	3	Livingstone thrust unit/location 8	VR	1.1	7	1.09	KTNY	8675
2-12	1	well 06-15-005-02W5	Tmax	457	7	1.08	KTNY	8675
3-10	3	Livingstone thrust unit/location 9	VR	1.1	8	1.12	KTNY	8675
3-11	3	Livingstone thrust unit/location 10	VR	1.1	7	1.09	KTNY	8675
1-39	1		Tmax	492	13	1.78	KTNY	8675
3-12	3	Livingstone thrust unit/location 11	VR	1.0	7	1.00	KTNY	8675
2-9	2	well 02-16-005-02W5	Tmax	471	11	1.43	KTNY	8675
2-8	2	well 02-16-005-02W5	Tmax	444	3	0.68	KTNY	8675
3-6	3	Turtle Mountain Thrust unit/location	VR	1.1	7	1.09	KTNY	8675
3-5	3	Turtle Mountain Thrust unit/location 4	VR	1.2	8	1.15	KTNY	8675
3-2	4		VR	1.08	7	1.08	MMTN	8675
1-44	1	Lodgepole	Tmax	605	19	3.75	KTNY	8675
3-1	4		VR	0.74	4	0.74	MMTN	8675
3-24	6	Coal Creek Mountain	VR	1.0	7	1.01	MMTN	8675
3-14	3	Livingstone thrust unit/location 13	VR	1.0	7	1.04	KTNY	8675
1-13	1		Tmax	438	2	0.53	MMTN	8675
1-19	2	well 02-01-005-02W5	Tmax	462	9	1.23	KTNY	8675
1-45	1	Lodgepole	Tmax	486	12	1.68	KTNY	8675
1-20	1	Livingstone thrust unit/Bellevue	Tmax	447	4	0.73	KTNY	8675
2-18	2	02-01-005-02W5	Tmax	447	4	0.73	KTNY	8675
3-22	6	Morrissey Ridge	VR	1.7	13	1.65	MMTN	(null)
3-13	3	Livingstone thrust unit/location 12	VR	1.0	7	1.02	KTNY	8675
3-54	3	Fernie Basin E./Corbin Mammoth seam 2	VR	1.1	8	1.14	KTNY	8675
3-15	3	Livingstone thrust unit/location 14	VR	1.1	7	1.07	KTNY	8675
3-57	4	well 06-14-008-05W5	Tmax	475	11	1.44	KTNY	8680
3-36	6	Sparwood Ridge	VR	1.3	9	1.27	MMTN	8695
3-55	4	well 06-14-008-05W5	Tmax	465	9	1.28	KTNY	8727
3-54	4	well 06-14-008-05W5	Tmax	461	8	1.18	KTNY	8751
3-53	4	well 06-14-008-05W5	Tmax	467	10	1.32	KTNY	8774
3-21	6	Morrissey Ridge	VR	1.9	15	1.85	MMTN	8775
3-19	6	Morrissey Ridge	VR	1.7	13	1.69	MMTN	8775
3-23	6	Coal Creek Mountain	VR	1.3	10	1.33	MMTN	8775
3-31	6	Natal Ridge	VR	1.3	9	1.28	MMTN	8775
3-34	6	Michel Creek	VR	1.6	12	1.56	MMTN	8775
3-37	6	Sparwood Ridge	VR	1.4	11	1.43	MMTN	8775
3-32	6	Michel Creek	VR	1.4	11	1.38	MMTN	8775
3-33	6	Michel Creek	VR	1.4	11	1.40	MMTN	8775
51	4	well 06-14-008-05W5	Tmax	461	8	1.18	KTNY	8821
50	4	well 06-14-008-05W5	Tmax	461	8	1.18	KTNY	8845
93	4	well 06-14-008-05W5	Tmax	492	13	1.68	FRNI	8857
255	4	well 07-34-003-01W5	Tmax	450	5	0.83	PGBD	8863
217	4	well 07-34-003-01W5	Tmax	446	4	0.74	PGBD	8867
254	4	well 07-34-003-01W5	Tmax	450	5	0.83	PGBD	8877
90	4	well 06-14-008-05W5	Tmax	461	8	1.18	FRNI	8882
271	4	well 07-34-003-01W5	Tmax	457	7	1.08	PGBD	8885
89	4	well 06-14-008-05W5	Tmax	464	9	1.28	FRNI	8891
253	4	well 07-34-003-01W5	Tmax	453	6	0.93	PGBD	8891

Table 1. (continued)

			OMR				Lithostratigraphic	
Code	Source[a]	Locality	Type	Rank	Category	VR[b]	Unit[c]	Approximate Depth[d] (m)
216	4	well 07-34-003-01W5	Tmax	447	4	0.74	PGBD	8903
252	4	well 07-34-003-01W5	Tmax	446	4	0.74	PGBD	8905
185	4	well 07-34-003-01W5	Tmax	442	3	0.66	PGBD	8910
251	4	well 07-34-003-01W5	Tmax	437	2	0.58	PGBD	8919
85	4	well 06-14-008-05W5	Tmax	474	11	1.44	FRNI	8924
275	4	well 07-34-003-01W5	Tmax	451	5	0.83	GBJC	8956
192	4	well 07-34-003-01W5	Tmax	441	3	0.62	GBJC	8968
2-10	2	well 02-16-005-02W5	Tmax	466	10	1.33	FRNI	8975
2-6	2	well 07-27-006-03W5	Tmax	487	12	1.68	FRNI	8975
2-11	2	well 06-15-005-02W5	Tmax	443	3	0.63	FRNI	8975
3-219	4	well 07-34-003-01W5	Tmax	442	3	0.66	GBJC	8982
3-277	4	well 07-34-003-01W5	Tmax	452	5	0.88	GBJC	8986
3-189	4	well 07-34-003-01W5	Tmax	436	2	0.58	GBJC	8991
3-76	4	well 06-14-008-05W5	Tmax	467	10	1.32	FRNI	9006
3-74	4	well 06-14-008-05W5	Tmax	469	10	1.36	FRNI	9023
3-73	4	well 06-14-008-05W5	Tmax	477	12	1.48	FRNI	9031
3-71	4	well 06-14-008-05W5	Tmax	469	10	1.36	FRNI	9048
3-67	4	well 06-14-008-05W5	Tmax	457	7	1.08	FRNI	9081
3-66	4	well 06-14-008-05W5	Tmax	464	9	1.28	FRNI	9089
3-65	4	well 06-14-008-05W5	Tmax	465	9	1.28	FRNI	9097
1-42	1	Lodgepole	Tmax	482	12	1.63	SPRR	9200
3-319	4	well 07-34-003-01W5	Tmax	438	2	0.58	LVGS	10391
3-313	4	well 07-34-003-01W5	Tmax	452	5	0.88	LVGS	10441
3-62	7	well 7-27-6-3W5	VR	1.2	8	1.16	EXWB	10650
3-71	7	well 07-27-006-03W5	VR	1.2	9	1.23	EXWB	10650
3-74	7	well 07-27-006-03W5	VR	1.1	7	1.08	EXWB	10650
3-73	7	well 07-27-006-03W5	VR	1.2	8	1.16	EXWB	10650
3-60	7	well 07-27-006-03W5	VR	2.0	16	1.96	EXWB	10650
3-63	7	well 07-27-006-03W5	VR	1.1	8	1.12	EXWB	10650
3-72	7	well 07-27-006-03W5	VR	1.30	10	1.30	EXWB	10650
3-69	7	well 07-27-006-03W5	VR	2.2	17	2.24	EXWB	10650
3-70	7	well 07-27-006-03W5	VR	1.6	12	1.56	EXWB	10650
3-75	7	well 07-27-006-03W5	VR	1.30	10	1.30	EXWB	10650
3-61	7	well 07-27-006-03W5	VR	2.1	17	2.11	EXWB	10650
3-66	7	well 07-27-006-03W5	VR	3.0	19	3.02	EXWB	10650
3-68	7	well 07-27-006-03W5	VR	1.2	8	1.15	EXWB	10650
3-65	7	well 07-27-006-03W5	VR	2.0	16	1.95	EXWB	10650
3-64	7	well 07-27-006-03W5	VR	1.6	12	1.61	EXWB	10650
3-67	7	well 07-27-006-03W5	VR	1.7	14	1.73	EXWB	10650
3-78	7	well 08-20-004-01W5	VR	2.10	17	2.10	EXWB	10650
3-58	7	well 07-27-006-03W5	VR	2.1	17	2.11	EXWB	10650
3-77	7	well 08-20-004-01W5	VR	1.70	14	1.70	EXWB	10650
3-79	7	surface sample Crowsnest	VR	1.30	10	1.30	EXWB	10650
3-76	7	well 08-20-004-01W5	VR	2.1	17	2.07	EXWB	10650
3-59	7	well 07-27-006-03W5	VR	2.2	17	2.16	EXWB	10650
3-62	7	well 07-27-006-03W5	VR	1.2	8	1.16	EXWB	10650
3-71	7	well 07-27-006-03W5	VR	1.2	9	1.23	EXWB	10650
3-79	7	Crowsnest	VR	1.30	10	1.30	EXWB	10700
3-58	7	well 07-27-006-03W5	VR	2.1	17	2.11	EXWB	10700
3-76	7	well 08-20-004-01W5	VR	2.1	17	2.07	EXWB	360
3-80	7	surface sample Crowsnest	VR	1.5	11	1.45	EXWB	10700
3-77	7	well 08-20-004-01W5	VR	1.70	14	1.70	EXWB	360
3-78	7	well 08-20-004-01W5	VR	2.10	17	2.10	EXWB	10700
2-7	2	well 07-27-006-03W5	Tmax	597	18	3.35	EXSW	10750
1-34	1	Crowsnest Pass	Tmax	568	18	3.10	EXSW	10750
1-33	1	Crowsnest Pass	Tmax	466	9	1.28	EXSW	10750
3-81	7	South Lost Creek	VR	1.9	15	1.85	WDBD	11400
3-45	7	Devonian	VR	1.4	11	1.41	WDBD	11400
3-44	7	Devonian	VR	1.5	12	1.54	WDBD	11400
3-81	7	South Lost Creek	VR	1.54	12	1.54	WDBD	11400

[a]Sample sources are (1) this study surface sampling, (2) this study well cuttings (3) *Hacquebard and Donaldson* [1974], (4) P. R. Fermor (personal communication, 2005), (5) *Stasiuk et al.* [2002], (6) *Pearson and Grieve* [1985], (7) *Stasiuk and Fowler* [2002].

[b]Vitrinite reflectance equivalent value.

[c]Units: PCPL, Porcupine Hills; WLCK, Willow Creek; SMRR, St. Mary River; BLRV, Belly River; ABGP, Alberta Group; WPIB, Wapiabi; SSPK, second White Specks; BLCK, Blackstone; BMGP, Blairmore; MNVL, Mannville; CDMN, Cadomin; KTNY, Kootenay; MMTN, Mist Mountain; FRNI, Fernie; PGBD, Passage Beds; GBJC, grey beds, Jurassic; SPRR, Spray River; LVGS, Livingstone; EXWB, Exshaw-Wabamun; EXSW, Exshaw; WDBD, Woodbend.

[d]Synthetic stratigraphic depth.

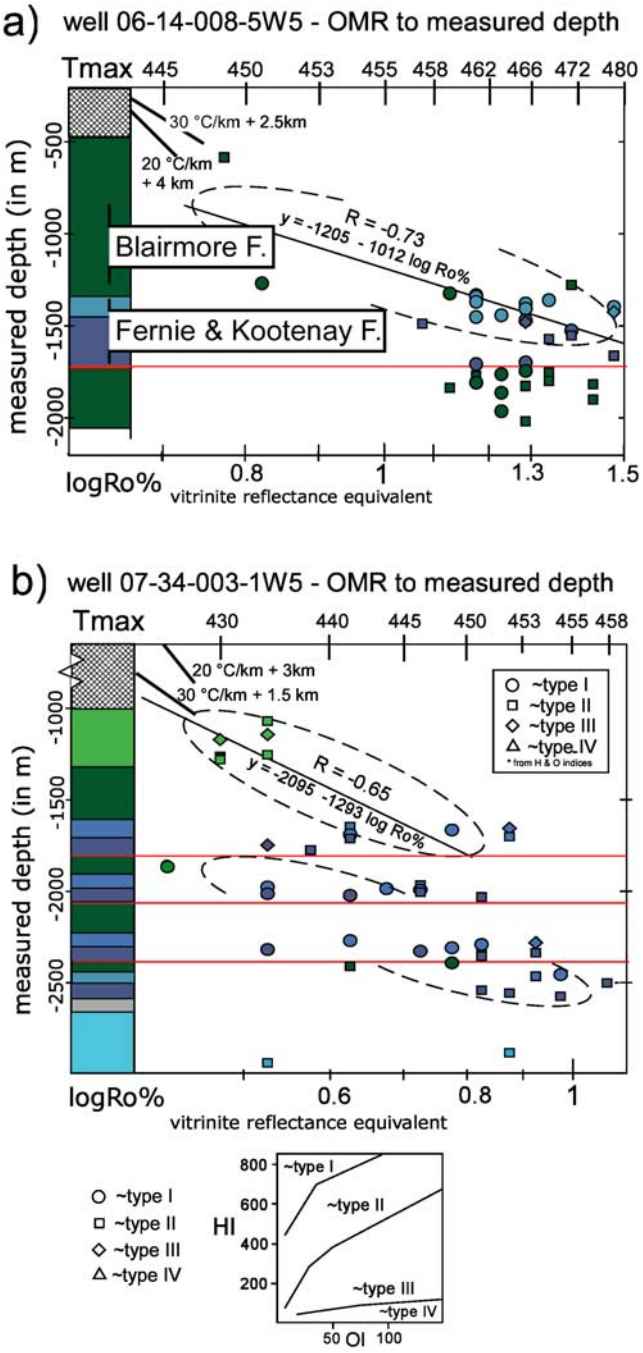

Figure 5. Organic maturity ranks for wells (a) 06-14-008-05W5 and (b) well 07-34-003-1W5. Along the horizontal log axis, vitrinite reflectance ranks (Ro) are plotted and correlated to corresponding Tmax values. Along the vertical axis, measured depth along well path together with its stratigraphy and interpreted positions of thrusts from stratigraphic duplications. The samples in both Figures 5a and 5b come with a kerogen characterization from hydrogen (HI) versus oxygen (OI) ratios.

sedimentary burial but also tectonic overburden has influenced the maturation history.

[32] The effect of syndeformational maturation can be further assessed following Hilt's Law that compares layer-perpendicular OMR gradients (i.e., to stratigraphic depth) with layer-parallel trends [e.g., *Pearson and Grieve*, 1985]. Positive correlation of the first implies a strong sedimentary burial imprint on the OMRs, whereas layer-parallel variations in OMR across different structures would indicate a syndeformation and postdeformation effect on the maturation history. For the Fernie Basin, *Pearson and Grieve* [1985] applied the Hilt's law by considering the layer-parallel and layer-perpendicular coalification gradients and denoted significant layer-parallel variability in OMRs across the Fernie Basin. They estimated 25–40% of postfolding coalification for OMRs of 1.0–1.4%Ro in the north (Natal and Sparwood ridges) to 75% of postfolding coalification for samples with ranks of 1.3–1.6%Ro south of Morrisey ridge (see Figures 3 and 4). This indicates a southward increasing importance of tectonic burial. In the MacDonald Range farther to the south (Figure 2), our samples give among the highest observed ranks for Kootenay coals in the study area (Figures 3 and 4) with Tmax values of more than 500°C that correspond with 1.8%Ro.

[33] Last, we give OMRs plotted onto a restored structural cross section (Figure 7). The profile gives the retrodeformed Fernie Basin and Turtle Mountain duplex system (see Figure 4a for structural cross section) along with OMR samples placed to their original stratigraphic and structural position, prior to their displacement. The samples from the Blairmore in the Fernie Basin show higher ranks than those from the foothills. It again illustrates that across different structural entities, OMRs from the same stratigraphic intervals yield different rank values.

[34] Finally, the importance of tectonic loading is also documented by *England and Bustin* [1986a], *Kalkreuth and Langenberg* [1986], *Kalkreuth et al.* [1989], and *Langenberg et al.* [1998] with clear examples of higher OMRs in some footwall blocks of significant thrusts in the area. We thus conclude that simple correlation to stratigraphic depth, as from organic maturation by sedimentary burial, does not fit with the OMR distribution in these highly imbricated thrust sheet stacks. Instead, it suggests that tectonic burial must have had at least some role in the maturation history of the above discussed samples.

[35] While the previous discussion documents the importance of tectonic burial in controlling the maturation history, various samples from the Lewis thrust footwall in the Cate Creek structural window (Figure 3), show low ranks at odds with what may be expected from an evident tectonic load. Despite the 5–6 km of overburden, which the Lewis thrust sheet presumably held after emplacement till Eocene times, samples show relatively low ranks with VR values of ~1%Ro (Figure 4c; ~455°C Tmax) [e.g., *Osadetz et al.*, 2004; *Hardebol et al.*, 2007]. Also in comparison of the ranks from wells 6-14-8-5W5 and 7-34-3-1W5, we already noted the low OMR values for the latter, even though the samples are overlain by a thin veneer of a presumably much thick Lewis thrust sheet.

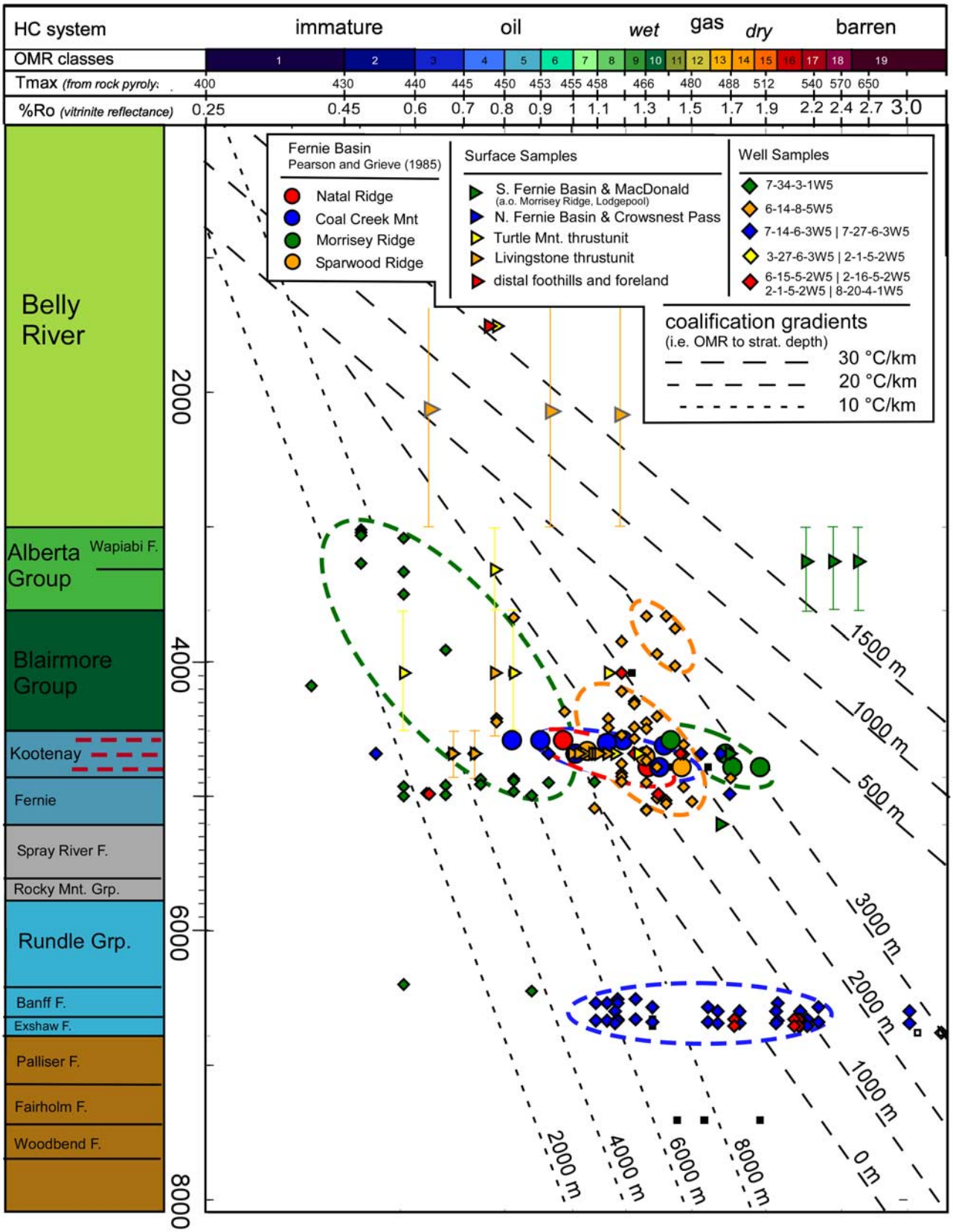
HC system
immature
oil
wet gas
dry gas
barren
OMR classes
Tmax (from rock pyroly:
%Ro (vitrinite reflectance)
Belly River
Alberta Group
Wapiabi F.
Blairmore Group
Kootenay
Fernie
Spray River F.
Rocky Mnt. Grp.
Rundle Grp.
Banff F.
Exshaw F.
Palliser F.
Fairholm F.
Woodbend F.
Fernie Basin
Pearson and Grieve (1985)
Natal Ridge
Coal Creek Mnt
Morrisey Ridge
Sparwood Ridge
Surface Samples
S. Fernie Basin & MacDonald
(a.o. Morrisey Ridge, Lodgepool)
N. Fernie Basin & Crowsnest Pass
Turtle Mnt. thrustunit
Livingstone thrustunit
distal foothills and foreland
Well Samples
7-34-3-1W5
6-14-8-5W5
7-14-6-3W5 | 7-27-6-3W5
3-27-6-3W5 | 2-1-5-2W5
6-15-5-2W5 | 2-16-5-2W5
2-1-5-2W5 | 8-20-4-1W5
coalification gradients
(i.e. OMR to strat. depth)
30 °C/km
20 °C/km
10 °C/km
1500 m
1000 m
500 m
3000 m
2000 m
1000 m
0 m
2000 m
4000 m
6000 m
8000 m
2000
4000
6000
8000

Figure 6

[36] Therefore, our OMR data set gives indication for both sedimentary and tectonic burial signal, but does not show a regionally consistent favor of one over the other. Different from earlier work, this study considers the maturation history the product of sedimentary and tectonic burial, particularly for the foothills located at the interface between foredeep deposition and thrust belt contraction.

3.4. Coalification and Paleotemperature Gradients

[37] Paleotemperature gradients can be inferred from coalification gradients as shown in many burial history studies [e.g., *England and Bustin*, 1986b; *Kalkreuth and McMechan*, 1988]. A linear increase of OMR ranks to stratigraphic depth describes the coalification gradient. Its slope yields information on the paleotemperature gradient and intercept with the 0.25% Ro isoline provides a rough estimate of maximum burial. Linear coalification gradients testify a relatively simple, mainly sedimentary burial history that involves steady paleotemperature conditions. Coalification gradients from wells for the undeformed foreland basin show such good correlation [e.g., *England and Bustin*, 1986b; *Kalkreuth and Mcmechan*, 1988; *Bustin*, 1991].

[38] Combining our new samples with OMR data sets from different previous studies of the FFTB, we find that OMRs correlate poorly with coalification gradients (Figure 6). We have plotted the OMR data together with a set of coalification gradients that are calculated from forward synthetic burial histories that contain different peak sedimentary burial depths and paleotemperature gradients. Comparison of these synthetic coalification gradients, with the OMR ranks from for instance well 7-34-3-1W5, may indicate a temperature profile of 20–30°C km^{-1} and ~2 km of overburden as best fit. Also the ranks from well 6-14-8-5W5 may trend around a coalification gradient with a comparable slope (i.e., temperature gradient), but the OMR values require higher overburden. The data cluster of well 6-14-8-5W5 is off-set what reflects the different structural position the samples hold (hanging wall versus footwall blocks). As earlier denoted, well 7-34-3-1W5 is currently overlain by a thin veneer of a formally much thicker Lewis thrust sheet, and the OMRs were regarded relatively low. The ~2 km of overburden, derived from extrapolation of the coalification gradient, shows insufficient to account for tectonic load of a formerly much thicker LTS.

[39] Deriving coalification gradients and estimating overburdens by upward extrapolation probably work for the undeformed basin where burial evidently occurred by sedimentary loading. Instead, obtaining linear coalification gradients and overburden estimates for the FFTB is hampered when the tectonic burial component is substantial.

[40] Inferred paleotemperature gradients form a first-order estimate of the geothermal conditions with presumably some regional application. As shown above, paleotemperature gradients can be inferred over a vertical stratigraphic section. Evidently, this inferred gradient is only regionally significant when temperature perturbations can be neglected. Another difficulty with inferred paleotemperature gradient occurs when not obtained over a specified stratigraphic interval. Sometimes the stratigraphic depth interval over which the gradient is estimated comprises a removed sedimentary section. Then, the estimated paleotemperature gradient contains a derived stratigraphic thickness which inherits a priori burial history assumptions. For instance, *Currie and Nwachukwu* [1974] and *Magara* [1976] provided respectively estimates of 20–25°C km^{-1} and 35–40°C km^{-1} from the same data set from the foreland basin, but considered different restored overburden thicknesses for the conversion. Thus, gradients estimated over a factual stratigraphic section, apply first to that specific interval and only when local anomalies show insignificant can be given more regional significance in forward burial history appraisal, whereas other estimates that contain inherent overburden assumption are better not considered. From our and previous findings [*Osadetz et al.*, 1992, and references therein], we consider a paleotemperature gradient of about 20–30°C km^{-1} as respectable regional average for the FFTB during its sedimentary and tectonic loading and exhumation history.

3.5. Deviations in OMR Trends and Paleotemperature Anomalies

[41] A combination of sedimentary burial and tectonic loading explains the distribution in OMRs that we find in our data set at first order, while significant departures remain from such first-order trends.

[42] First, it is worth noting that scatters in OMR distribution can occur by the slightly different kinetic response that different organic matter types (i.e., the kerogen type) exhibit to similar temperature evolutions. Without going into detail on organic maturation kinetics [see, e.g., *Espitalié*, 1986], kerogens with lower hydrogen index (i.e., type II versus type III) can give slightly higher ranks. Many new samples in our data set comprise Tmax from rock pyrolyses data, having hydrogen and oxygen ratios that disclose kerogen type. Figures 5a and 5b include a rough OI/HI characterization and show that the scatter contains indeed higher ranks for the kerogens of lower HI. It shows how 0.2 log % Ro and 5–10°C in Tmax scattering can be the results kerogen type differences, thus setting the precision with which geologic trends in our OMR data set can be made.

[43] Furthermore, some OMR data call for other explanations than sedimentary or tectonic burial and fall beyond the scattering from kerogen-type. Samples from the MacDonald Range, at the southwestern rim of the Fernie Basin have the highest values for the study area. Within this range, partic-

Figure 6. Organic maturity ranks plotted along a pseudostratigraphic column. The plot summarizes the bulk of the OMR data; a few values represent averaged values of combined, closely spaced samples. Most samples come from the Jurassic Fernie to Cretaceous Alberta Group from across the study area and are classified to their localities (i.e., wells or structural entities). Along with the ranks, theoretical OMR gradients are plotted illustrating the effect of increasing stratigraphic burial and different geothermal gradients. Higher paleotemperature gradients give an increasing slope, whereas increasing depth of burial offsets the OMR gradient [after *Bustin*, 1991].

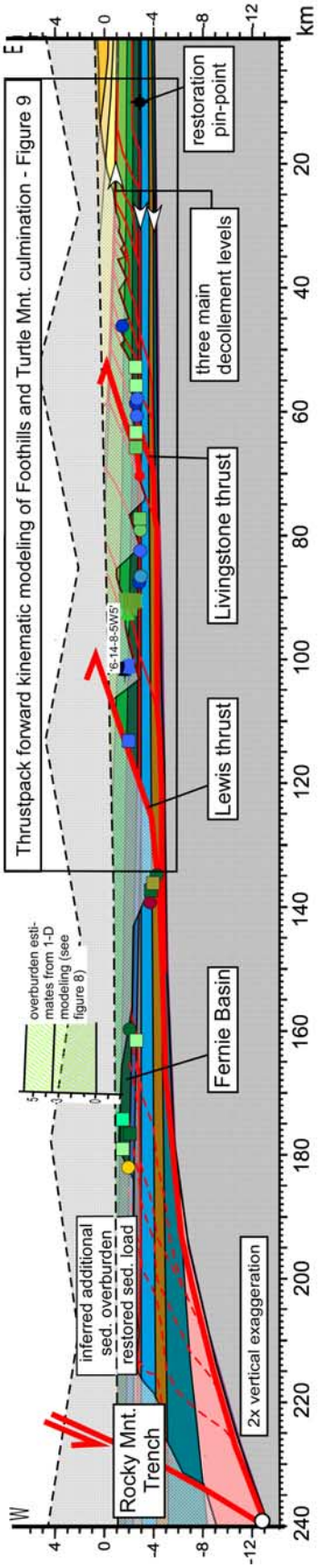

Figure 7. Restored cross section for profile A (Figure 4a) including the retrodeformed Fernie Basin, the Lewis thrust sheet, and restored thrust sheet stacks of the Turtle Mountain duplex system (i.e., Turtle Mountain and Livingstone thrust sheets). Also, the erosion profile is shown outlining the restored sedimentary load and additional overburden prior to the contraction of the belt.

ularly high values with Tmax of 500°C can been found for samples in the Howell Creek structure (see Figures 3 and 6). These high Tmax values are especially significant when considering their stratigraphic shallow position in the Late Cretaceous Alberta Group (i.e., the upper Alberta Wabiabi Formation). At first glance, the structure shows resemblance to the exposed Cretaceous sediments in the footwall of LTS of the nearby Cate Creek window, suggesting the occasion of tectonic loading. However, the Howell Creek structure, although once regarded a structural window exposing the LT footwall, is since long considered a down-faulted slice of the Lewis thrust hanging wall [*Labrecque and Shaw*, 1973]. Sedimentary nor tectonic loading can explain the extremely high OMR values for the samples of this structure, and the only explanation the structure leaves are the presence of Late Cretaceous intrusives that must have caused a local temperature anomaly.

[44] Another collection of samples with deviating ranks come from the Mississippian carbonates, at the bottom of the synthetic stratigraphic chart (Figure 6). These samples depict a wide scatter of Tmax values between 450 to 550°C. They come from various wells close to the Turtle Mountain duplex in the foothills (i.e., wells 8-20-4-1W5, 7-20-6-3W5, and 7-27-6-3W5; Figure 4) that sample especially the autochthonous underneath the foothills basal decollement. The samples from the three wells group within a small stratigraphic interval (Figure 4) in a single structural entity, and the spread in Tmax values highlight an anomaly from the first-order sedimentary and tectonic burial trends. The amount of samples and the width of the scatter make the anomaly significant enough and the fact that the rocks forms a fluid flow conduit, may have an influence on the OMR values. That fluid flow can affect organic maturation history is suggested only in few studies where 0.4%Ro in OMR variability was found, introduced by local thermal perturbation from episodic hot groundwater flow [*Lampe et al.*, 2001; *Lampe and Person*, 2002]. Also in the study area, a stable isotope study pointed to local temperature anomalies from fluid circulations through the thrust sheets [*Cooley et al.*, 2006]. Various studies have better examined the effect from fluid flow [e.g., *Forster and Smith*, 1989; *Bodri and Rybach*, 1998] and also of denudation [*Mancktelow and Grasemann*, 1997; *Stuwe and Hintermuller*, 2000] for the temperature evolution in mountainous areas. In this study we concentrate on the kinematics of burial and temperature history appraisal.

4. Thermokinematics of Strongly Deformed and Denudated FFTB

4.1. Thermokinematic Principles in Thrust Belt Systems

[45] Where OMR data help the examination of different overburdens backward in time, forward thermokinematic models can predict OMR distributions in response to burial histories by including appropriate organic maturation kinetics [e.g., *Tissot et al.*, 1987; *Sweeney and Burnham*, 1990]. Also, forward models test in how far the temperature field might have evolved along with the burial and deformation history. Coupled thermokinematic models can address the effect that sedimentary burial, fault block motions and consequent exhumation have on the evolution of the temperature field.

[46] Many previous forward thermokinematic models regarded heat advection from a few thick-skinned thrust sheets at large, often orogenic scales [*England and Thompson*, 1984; *Ruppel and Hodges*, 1994]. Since then, the influence of thrust displacements in combination with an eroding topography on the temperature evolution has been well addressed [*Stuwe and Hintermuller*, 2000; *Moore and England*, 2001; *ter Voorde et al.*, 2004]. More recently, forward thermokinematic models have been utilized to examine burial and temperature histories of complex thrust belt systems [e.g., *Sassi et al.*, 2007; *Lock and Willett*, 2008], and applied to the petroleum system prospects [*Faure et al.*, 2004; *Deville and Sassi*, 2006]. Different from crustal-scale thermokinematics, temperature fluctuations in a FFTB with thin-skinned moderate thrust sheet displacement rates are considered more subtle [*Ehlers and Farley.*, 2003; *Husson and Moretti*, 2002].

[47] Heat advection prevails when heat diffusion cannot keep pace with the translation of isotherms from material transport. In a FFTB system, heat advection introduces temperature perturbations when thrust sheet stacking or sedimentary burial occur fast enough to prevent the thermal field to readjust with equal pace. The amount of temperature perturbation (i.e., transient heat effect) results primarily from effective displacement (i.e., vertical motions) and denudation rates [e.g., *Mancktelow and Grasemann*, 1997]. Only under conditions of sufficiently vast effective vertical motions, heat affection and perturbation of the temperature field might occur [*Endignoux and Wolf*, 1990; *ter Voorde et al.*, 2004; *Sassi et al.*, 2007].

[48] Coupled thermokinematic models of complex FFTB systems rely strongly on the description of the material displacement field and heat transfer through the deforming wedge. The displacement fields of the particles in the model are a function of the fault block geometries, detachment surfaces and the amounts and relative timing of the displacements along the different faults. The material displacement field of an actively deforming FFTB prism is further controlled by the basement flexure and denudation at surface.

[49] Thermokinematic models that include realistic definition of fault block motions can determine the temperature evolution of particles in the belt as induced by the deformation history of the thrust belt. Along with temperature histories, organic maturation and fission track annealing can be calculated. Also, coupling temperature calculations to a semirealistic kinematic scenario can predict whether spatial or temporal variations in the temperature field occurred during the deformation.

4.2. Modeling Approach

4.2.1. Thermokinematic Modeling Strategy

[50] The thermokinematic model comprises a portion of the FFTB that is the foothills around the Turtle Mountain duplex system, i.e., the eastern half of the northernmost of our structural cross sections (see Figures 3 and 4a).

[51] The foothills form a transition which burial history combines sedimentary and tectonic loading. East of the

Table 2. Thermal Rock Parameters Used in Thrustpack Forward Thermokinematic Modeling for the Scenario in Figure 8[a]

Parameter	Formulations or Values
Porosity of sediments	$\phi = \phi_0(z)$ with ϕ_0 the reference porosity of given sediment type
Heat capacity	$C_p \sim 1100$ J kg^{-1} K^{-1}, i.e., also dependent on sediment type and porosity
Thermal conductivity	$k = k_s^{(1-\phi)} k_w^{(\phi)}$ with k_s and k_w the heat capacities of sediments and water, respectively
Thermal diffusivity	$\kappa = k/\rho C_p$ with resulting values for limestone 1.0×20^{-6}, sand siltstones 0.7×10^{-6} to 1.5×10^{-6}, and shales 3.0×10^{-7} to 8.0×10^{-7} m^2 s^{-1}
Boundary conditions	Heat flux at base box 50 mW m^{-2}; Surface temperature 20°C

[a]See *Sassi et al.* [2007] for further explanation.

foothills, the burial of the undeformed foreland basin comprises pure sedimentary loading. West of the foothills, the FFTB contains thicker thrust sheets, comprising Mesoproterozic and lower Paleozoic sequences, whereby the Late Cretaceous–Paleocene burial history occurred predominantly by tectonic loading. Located at this transition, modeling of the Turtle Mountain foothills portion allows well to study the interaction between tectonic and sedimentary loading.

[52] First, we describe the retrodeformed cross section of the foothills, which will later be used as the initial stage for the forward kinematic modeling. Although most thrust sheet motions in the foothills occurred in Paleocene time (Figure 2c), the preceding Campanian loading under Belly River sediments forms a critical part of the burial history as well. We decided to examine first the thickness of this Belly River overburden with some 1-D burial history modeling. The estimated Belly River load is added to the structural restored cross section to outline the sedimentary wedge, which the foothills comprised in Campanian time prior to its contraction. Subsequently, the 2-D thermokinematic model test in how far this sedimentary loading combined with the tectonic loading achieves the required peak burial and temperatures for Paleocene times.

[53] For the 1-D burial history modeling, we used the Genex® burial modeling software [e.g., *Faure et al.*, 2004] and performed a sensitivity test varying upper Cretaceous overburdens. While Genex can account for a tectonic load, evidently, the sequential and lateral motions of multiple thrust sheets cannot be accounted for. Nonetheless, Genex modeling is helpful as it provides for fast testing of multiple simple burial history scenarios for Late Cretaceous times when the effect from thrust sheet loading was still small (Figure 2c). After the inspection of implications from Belly River overburdens, the 2-D forward thermokinematic modeling further examines the burial history, accounting much better for the tectonic loading that occurred in the foothills particularly in Paleocene time.

4.2.2. The 2-D Thermokinematic Model Setup

[54] Our study employs the integrated thermokinematic modeling environment Thrustpack [*Roure and Sassi*, 1995; *Sassi and Rudkiewicz*, 1999; *Sassi et al.*, 2007]. The modeling comprises an explicitly defined complex kinematic history scenario that examines the burial, temperature and OMR evolution. Rather than testing a variety of conceptual kinematic scenarios, this modeling focuses on a specified semi-realistic kinematic scenario to study what spatial trends and disparities in temperature history and consequent OMRs might be anticipated.

[55] The temperature calculations account for heat generation from radioactive decay whereas the effect from shear heating on the faults is not considered [*Barr and Dahlen*, 1989]. The thermal calculations comprise a thermal structure with a heat flow of 50 mW m^{-2} entering the base of the kinematic model domain and is constant through time (see also Table 2 for thermal parameterization). The differential heat equation is numerically solved with the generalized trapezoidal approach [*Hughes*, 1987; *Sassi and Rudkiewicz*, 1999; *Sassi et al.*, 2007].

[56] The deformation history for the Turtle Mountain foothills portion of the FFTB is described in 16 successive kinematic time steps, seven of which are shown in Figure 9a. For each time step, displacements are assigned to each individual fault block (i.e., timing and amounts), involving inferences from the structural balancing work [*Hardebol et al.*, 2007]. Flexural subsidence is imposed with a horizontal deflection profile applied across the basement block, in such a manner that the foredeep basin accommodates a sedimentary record in agreement with burial history studies [e.g., *Kalkreuth and McMechan*, 1988; *Bustin*, 1991] and that a curvature is maintained comparable with foreland flexure studies [*Beaumont*, 1981; *Peper*, 1993].

[57] The upper boundary of the model is formed by the paleotopography that contains zero elevation for the undeformed portion, and a westward stepwise increase in elevation from 500 to max. 1500 m. for the deforming wedge. For each time step, a paleotopography profile is defined that reflects the wedge shape for the contracted portion of the transect. Erosion and sedimentation are specified such that a smooth paleotopography profile is maintained and levels the surface distortions introduced by uplift and subsidence from the various fault block motions and down flexure of the basement. As such, the evolution of the contractional wedge is constrained by the basement down flexure and the topography as bounding geometries and by fault block geometries and motions that control the relative material pathways. By omitting undulations in topography of the evolving FFTB

wedge, lateral variations in exhumation history prediction of our model result exclusively from differences in fault block motions.

4.3. Restoring the FFTB to the Initial Stage

4.3.1. Retrodeformed Cross Section

[58] The structural cross section (Figure 4a) has been retrodeformed with the triangle zone footwall block as pin point in the east and is shown in Figure 7 [see also *Hardebol et al.*, 2007]. The restored thrust units involve three main decollement levels. The first in the Cambrian shales that involves thrust sheets scraped off from the undeformed basement. A second persuasive decollement level occurs in the Jurassic Fernie shales that requires restoration of the Mesozoic thrust sheets independent of the Paleozoic ones (see also *Hardebol et al.* [2007] for further discussion). A third decollement level retrodeformed in the cross section is located in the Bearpaw Formation at the base of the foredeep sequence under which the Mesozoic thrust sheet imbricates of the distal foothills of the triangle zone are restored.

[59] For the foothills portion of the FFTB, the Paleozoic and Mesozoic units are decoupled, which implies that also the retrodeformation is done independently. For the Lewis thrust sheet instead, the Mesozoic is considered more or less autochthonous to the underlying Paleozoic as the Mesozoic of the Fernie Basin was presumably deposited syntectonically, in a piggyback configuration atop of a deforming Lewis thrust sheet. This constraints the restoration of the Paleozoic and Mesozoic units of the foothills as they should give similar restored lengths in between the undeformed foreland basin block and the Lewis thrust sheet. The restored cross section (Figure 7) indeed gives similar restored lengths of ~120 km for both the Mesozoic and Paleozoic thrust units of the foothills. The foothills, which currently encompass a distance of ~40 km, thus accommodate a shortening of 70–80 km. The Lewis thrust itself accommodates about 15–25 km of shortening and displaces over a total distance of 85–100 km [see *Hardebol et al.*, 2007]. With this displacement and a duration of its activity over a 20 Ma time span (~78–58 Ma; Figure 2) [*van der Pluijm et al.*, 2006], the Lewis thrust sheet yields an average displacement rate of ~5 mm a^{-1}.

4.3.2. Estimates of Initial Sedimentary Load

[60] Along with the retrodeformation of the fault blocks, the cross section also provides an indication of the initial sedimentary load prior to the contraction of the belt. The Cretaceous sediments provide the initial burial load to the foothills, after which the tectonic load was added during Paleocene contraction (Figure 2c). In the Lewis thrust hanging wall, Cretaceous strata are only present at a few locations and restored thickness estimates of the removed overburden need to come from 1-D burial history modeling [*Hardebol et al.*, 2007].

[61] The Fernie Basin contains OMRs over a mid-Cretaceous stratigraphic interval that includes several coal seams. The present-day strata of the Fernie Basin comprise the Kootenay shales with several coal seams and are overlain by the middle Cretaceous Blairmore Group. Figure 7 shows the restored Fernie Basin, also depicting additional overburden that may be inferred from the OMRs and burial history modeling. We tested the amount of Belly River sedimentary overburden and duration that is required for the organic matter to reach their measured ranks. As example, Figure 8a shows four different burial history curves for a synthetic sample from one of the Kootenay coal seams. The four models yield different sedimentary burial loads, basal heat flow values (Figure 8b) and also the duration over which the burial load is preserved varies (Figure 8a). For the synthetic sample, we also show the temperature evolution through time resulting from the imposed burial history (Figure 8a). The depth interval between the 40, 80 and 120°C isotherms clearly change over time and depict the variation in paleotemperature gradient as result of the burial and exhumation history. Figure 8b gives estimated steady state and perturbed temperature gradient at time of peak burial. Last, Figure 8c shows calculated OMR values and coalification gradients, plotted along with measured OMRs from sampled profiles in the Fernie Basin [*Pearson and Grieve*, 1985].

[62] In models 1 and 3 peak burials are reached over a short Campanian time interval, prior to the onset of motion of the underlying Lewis thrust (i.e., before ~75 Ma; see Figure 2c for timing). Model 1 describes the history of a synthetic sample buried under 3.5 km of Campanian Belly River sediments with a basal heat flow of 50 mW m^{-2} that consequently reaches the measured OMRs fastly. Also for Model 3, the organic maturation achieves the measured rank prior to the emplacement of the Lewis thrust sheet by 5 km of Campanian Belly River sediments. In both cases, fast burial occurs over a short time span of less than 10 Ma with erosion following immediately after. As a consequence, the initial steady state temperature gradients drop with more than 10°C km^{-1} (Figure 8b). These scenarios thus achieve peak temperatures under strongly perturbed paleotemperature conditions, with a low coalification gradient as result (Figure 8c).

[63] Differently, models 2 and 4 reach peak burials over a more extended time span and establish a steady temperature with peak temperatures and OMR values, which fit measured ranks, reached at a later stage. Although these models do not account for thrust sheet displacements, it still shows that burial requires extended time over the duration of contraction in the belt.

[64] Hence, it is difficult to envision how samples in the Fernie Basin could have acquired the observed OMRs from purely sedimentary loading (by Belly River sediments) before the underlying Lewis thrust carried it to structural higher levels. Instead, thermal steady state conditions can be maintained when peak burial occurred as combination of sedimentary with tectonic loading.

[65] Compared with other studies [e.g., *Osadetz et al.*, 2004], we thus reduced the inferred Belly River overburden to 3 km and consider it being synchronous with the thrusting activity of the underlying Lewis thrust sheet. We further examine this scenario with 2-D thermokinematic modeling that contains much better the effect of displacement and loading from thrust sheets.

4.4. Forward 2-D Kinematic Scenario

[66] Our forward kinematic scenario describes the evolution of the foothills in 16 successive stages. The first stages

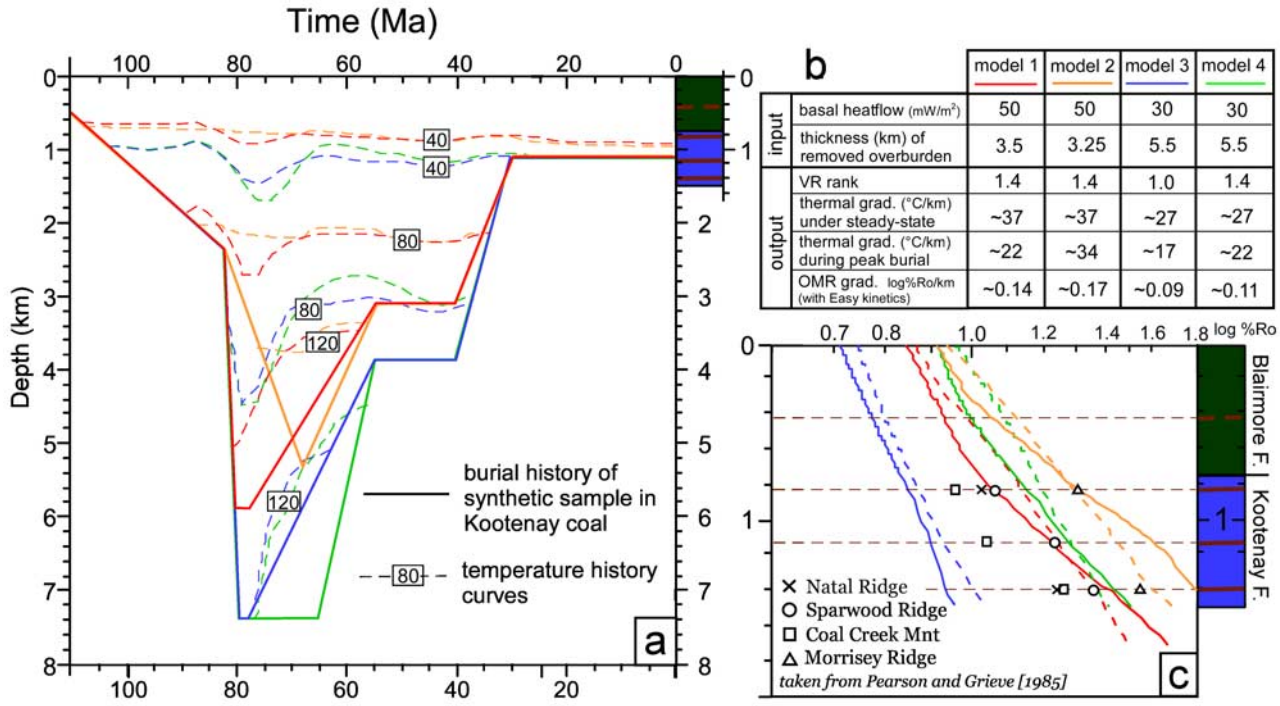

		model 1	model 2	model 3	model 4
input	basal heatflow (mW/m²)	50	50	30	30
input	thickness (km) of removed overburden	3.5	3.25	5.5	5.5
output	VR rank	1.4	1.4	1.0	1.4
output	thermal grad. (°C/km) under steady-state	~37	~37	~27	~27
output	thermal grad. (°C/km) during peak burial	~22	~34	~17	~22
output	OMR grad. log%Ro/km (with Easy kinetics)	~0.14	~0.17	~0.09	~0.11

Figure 8. One-dimensional well modeling from Fernie Basin, a summary from results presented by *Hardebol et al.* [2007], with four different burial and exhumation history scenario being tested. (a) Burial and thermal histories for synthetic sample in the middle Kootenay coal seam. (b) Table showing input and output values. (c) Calculated OMR gradients plotted against measured OMR values from the Fernie Basin.

describe the deposition of the Paleozoic succession; the Jurassic Fernie and Kootenay Formations followed by the Blairmore and Alberta Group in mid-Cretaceous time (see Figures 2b and 2c for timing). This way, our model describes the burial and organic maturation history also for the Devonian Exhaw shales starting off in Paleozoic time.

[67] The first motion in the model occurs along the Lewis thrust, that we name as kinematic stage I (at 75 Ma) and takes place outside the left margin of the display domain in Figure 9. The deposition of the Belly River Formation, that coalesces, shows a thickness of 3 km in the west and tapers eastward to 1 km as consequence of imposed tilted subsidence of the basement (Figure 9).

[68] Time stages II–IV (64–54 Ma) depict the main episode of foothills contraction, with displacement applied along the Lewis thrust and in-sequence activation of all main thrusts including the Livingstone thrust. Upthrusted sheets are eroded at their tips as we maintain the specified paleotopography profile.

[69] In time slice V at 45 Ma, most of the contraction in the FFTB and deposition in the basin (Porcupine Hills Formation) are completed. The deformed foothills have reached the present-day width (see Figure 4a, i.e., the present-day cross section for comparison), the triangle zone has accommodated the imbricated sheets under its roof thrust and tilted the proximal foredeep, which stores the inferred Paleocene maximum overburden.

[70] As we will explain, it is only at this point that the kinematic model releases the accumulated overburden (Figure 9a; slices V and VI; late Paleocene to Oligocene). The forward kinematic model contains ~3 km of postorogenic erosion in the proximal foredeep, and 3–5 km exhumation for the foothills. Furthermore, while the overall contraction has ceased in the belt, out-of-sequence displacement is considered for the Livingstone thrust, that is the roof thrust of the Turtle Mountain duplex system [*Hardebol et al.*, 2007].

[71] The final stages VII–VIII contain some minor Neogene erosion and show a forward modeled end stage that compares well to the present-day cross section of Figure 4a.

4.4.1. Considerations on Out-of-Sequence Thrusting and Postorogenic Exhumation

[72] The forward kinematic scenario contains the typical in-sequence activation of thrust sheets and get eroded at the exposed tips. The overall erosion in the FFTB, however, is limited because of strong basement down flexure. This Paleocene basement subsidence is attested for the undeformed basin at the eastern end of the model. Overburden studies for the basin require a thick Paleocene sedimentary burial load. The flexural curvature of the basement transfers the subsidence from the basin to the FFTB. The kinematic model (Figure 9) depicts clearly how the strong subsidence in the foredeep implies also the preservation of a thick wedge in the foothills, thus preventing significant synorogenic exhumation [*Sears*, 2001; *Osadetz et al.*, 2004; *Hardebol et al.*, 2007]. As a result, substantial tectonic overburden from thrust sheet stacking can pile up and be preserved (Figure 9; stage V at 45 Ma). It further follows that peak burials are

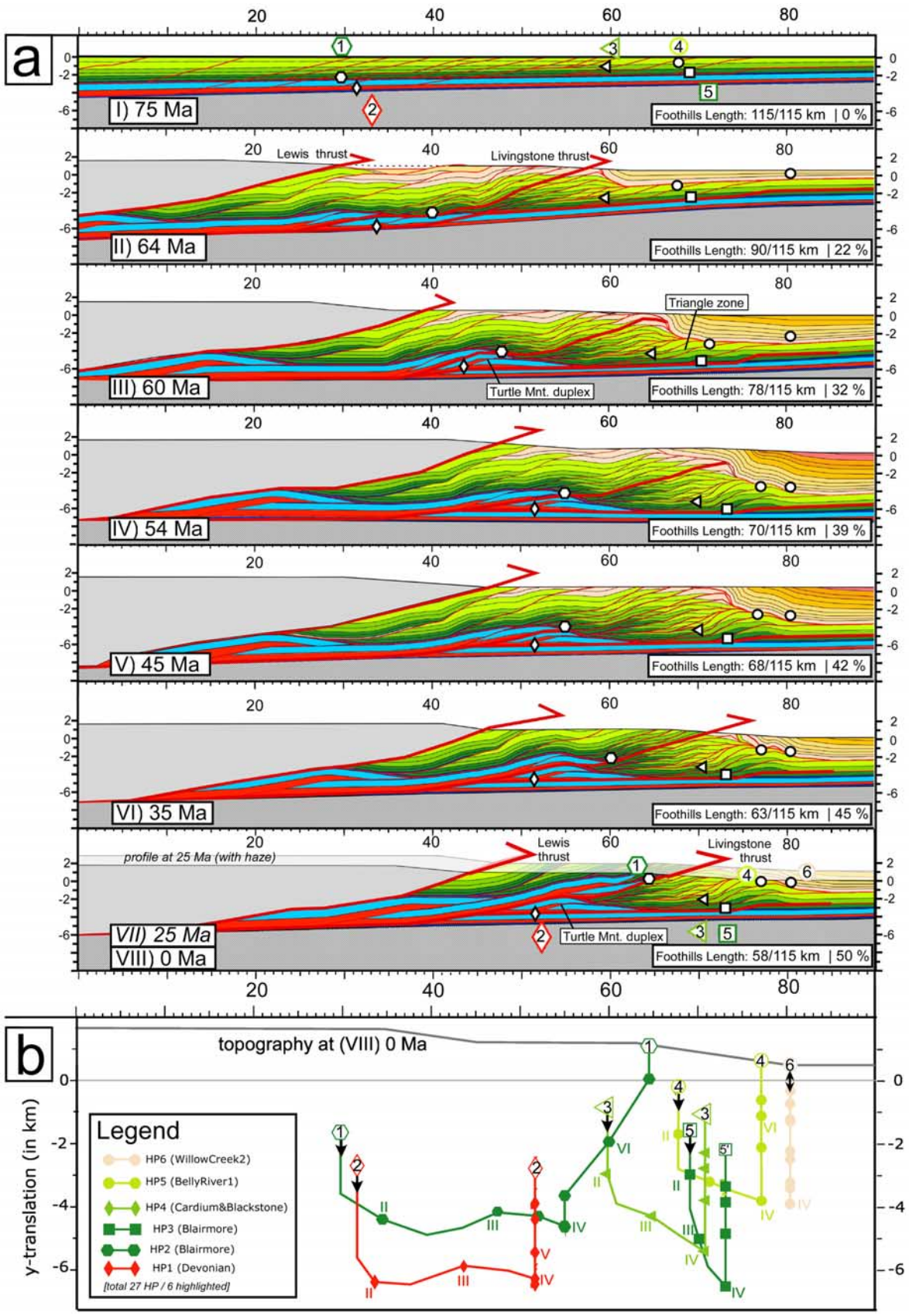
a
I) 75 Ma
Foothills Length: 115/115 km | 0 %
Lewis thrust
Livingstone thrust
II) 64 Ma
Foothills Length: 90/115 km | 22 %
Triangle zone
Turtle Mnt. duplex
III) 60 Ma
Foothills Length: 78/115 km | 32 %
IV) 54 Ma
Foothills Length: 70/115 km | 39 %
V) 45 Ma
Foothills Length: 68/115 km | 42 %
VI) 35 Ma
Foothills Length: 63/115 km | 45 %
profile at 25 Ma (with haze)
VII) 25 Ma
VIII) 0 Ma
Foothills Length: 58/115 km | 50 %
b
topography at (VIII) 0 Ma
y-translation (in km)
Legend
HP6 (WillowCreek2)
HP5 (BellyRiver1)
HP4 (Cardium&Blackstone)
HP3 (Blairmore)
HP2 (Blairmore)
HP1 (Devonian)
[total 27 HP / 6 highlighted]

Figure 9

reached in lower Paleocene times and not earlier by Belly River sediments in Campanian times.

[73] The model subsequently shows postorogenic exhumation of the foothills along with denudation of the undeformed basin and out-of-sequence motion along the Livingstone thrust. While activation of the Livingstone thrust sheet is defined in sequence with the other foothills thrusts, we consider late stage reactivation. This is required because the Paleozoic strata, carried by the Livingstone thrust, currently override imbricated Mesozoic thrust units, which they once underlay. The retrodeformed cross section (Figure 7) restores these Mesozoic thrust units atop of the Paleozoic of the Livingstone thrust sheet. The Paleozoic strata in the Livingstone thrust could only get emplace atop of the Mesozoic imbricated strata after major contraction of the foothills.

[74] It is important to readdress the fact that the Paleozoic thrust sheets are mostly decoupled from, and stay underneath the imbricated Mesozoic thrust units. During the main contraction of the foothills (stages II to V), the Paleozoic thrust sheets form duplex systems underneath a Mesozoic cover that accommodates the shortening by imbrication. Only after renewed motion along the Livingstone thrust, the fault cuts across the Fernie decollement and joins with Mesozoic imbricated thrust units.

[75] However, this more than 10 km motion of the Livingstone thrust sheet is hampered by the thick imbricated Mesozoic cover, and requires removal to support the motion. The overburden, which accumulated during the Paleocene in the undeformed basin, has since been removed and allowed reactivation of the Livingstone thrust coeval with large wavelength exhumation of the foothills and undeformed foredeep in post-Paleocene time.

4.4.2. Burial History Points

[76] The forward kinematic model provides the material pathways for a set of predefined tracking points that describes their burial and exhumation histories. Figure 9b shows horizontal and vertical displacement trajectories for six history points. They record the integrated response to burial from both sedimentation and thrust sheet stacking followed by erosion after the sheets reach surface. The maximum burial depth that samples can reach in the wedge is defined by the difference in amount of basement flexure and topography the system has created at a given time. The exhumation trajectory subsequent to the peak burial reflect the interplay between motion of the thrust sheet that carries the sample and denudation at the surface.

[77] The first history point (HP1; Figure 9b) is located in the middle Cretaceous Blairmore Formation, in the hanging wall of the Livingstone thrust. At time stage I, HP1 is buried under 2 km lower Paleocene sediments. In subsequent stages (between II and IV), the sedimentary load gets partly removed with the displacement of overlying thrust sheets, but HP1 remains buried as the tectonic load from thrust sheet stacks replaces the sedimentary load. Only after stage V, HP1 is brought to surface as the combined result of late stage motion of the Livingstone thrust and regional-scale exhumation. HP1 thus records a net 3 km vertical and 40 km horizontal translation, which gives a clear example of the combined effect of sedimentary burial, tectonic loading and exhumation.

[78] HP2 is located in the Devonian in one of the thrust slivers in the footwall of the Livingstone thrust. At stage I, HP2 is buried under 3 km of sediments including 2 km of the Belly River Formation. Like for HP1, the latest Cretaceous and earliest Paleocene mark fast burial under a combination of sedimentary and tectonic loading. With the motions of overlying thrust sheets, tectonic overburden replaces the sedimentary load between stages II and IV and HP2 records little exhumation during the contraction of the belt. Some postorogenic exhumation occurred associated with large wavelength basement involved uplift, bringing HP2 to its present depth at 4 km in the Turtle Mountain duplex system.

[79] HP3, HP4 and HP5 are all located in the more distal portion of the foothill. They record tectonic loading from imbricated thrust sheets beneath the triangle zone combined with sedimentary burial from the overlying foredeep sediments. The three HPs record post-Paleocene erosion (stages V to VIII) which reflect the associated exhumation of the foreland basin. The tilted foredeep sediments next to the

Figure 9. Forward thermokinematic modeling of the Turtle Mountain foothills section (see Figure 6a), showing the kinematic of the foothills from a series of successive time slices. (a) The kinematic evolution from 7 time slices: stage I at 75 Ma, deposition of Upper Cretaceous foredeep sediments (Belly River Formation in light green), just prior to onset of deformation in this portion of the foothills (0% shortening for foothills). Stage II at 64 Ma, with the Lewis thrust sheet encroaching from the west; contraction is introduced in the area. Stage III at 60 Ma, a triangle wedge is being formed from the interference of strong imbrication in the foothills and deposition in the foredeep. The foothills give a shortened length of 78 km (initial, restored length of 115 km) and 32% contraction. Furthermore, also the Turtle mountain duplex starts forming from Paleozoic thrust sheet stacking detached from the overlying Mesozoic series. Stage IV at 54 Ma, in Paleocene time, maximum burial is achieved both in the undistorted foredeep based on sedimentary loading and in the deformed belt by a mixture of sedimentary burial and loading from thrust sheets. Stage V at 45 Ma, contraction has seized in late Paleocene time with 42% shortening for the foothills (i.e., 68 km length relative to 115 km restored foothills length). Meanwhile, much of the overburden remains presumably preserved till late Eocene times. Stage VI at 35 Ma, at the end of an Eo-Oligocene exhumation phase that removed several kilometers of sediments, not only from the deformed FFTB but also from the undisturbed foreland basin areas. Out-of-sequence motions of the Livingstone thrust, as roof thrust of the Turtle Mountain duplex system, assumable occurred along with this exhumation and accumulates another $\sim$10 km shortening to a total of 50% contraction for the foothills. Stages VII and VIII between 25 and 0 Ma, in Neogene times, some remaining denudation occurs in the study area to present-day. (b) Plot depicting horizontal and vertical displacement histories for selected history points as result of the imposed kinematic history. Six history points (HPs) are highlighted.

deformation front get completely removed, whereby HP4, located at the crest of the antiformal stack, can reach surface. The other two history points remain buried under 2 km of imbricated thrust sheets of the former triangle zone.

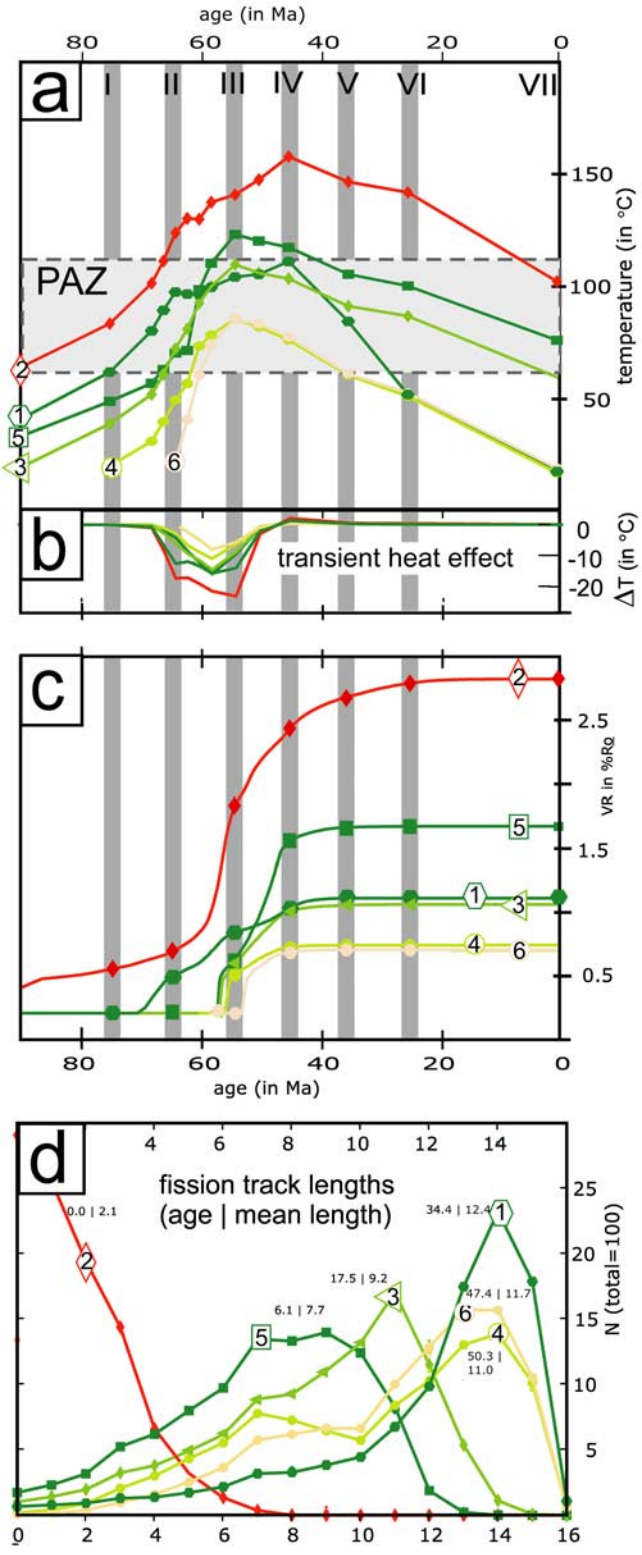

[80] HP6 is located within the undeformed foreland basin, east of the deformation front. Hence, it doesn't record horizontal translations and the burial is entirely controlled by sedimentary loading, with the postorogenic exhumation also clearly evidenced.

4.5. Forward Modeling Derivates

[81] The forward kinematic and burial exhumation model predicts temperature and organic maturation histories shown in Figure 10. The temperature calculations follow a steady state and transient heat equation that involves thermal diffusion and advection terms. Temperature history curves are given as outcome of the steady state and transient heat solution separately. The first gives the temperature history of material pathways through a stationary thermal field, whereas the transient solution shows the amplitude in temperature perturbations that the model generates.

[82] OMR predictions are calculated from the derived temperature evolution, choosing kinetic laws for organic matter transformation [*Ungerer et al.*, 1990; *Roure and Sassi*, 1995]. A simplified kerogen distribution of type II is applied across the model that allows for generic comparison with our OMR data set. Furthermore, the temperature histories for the different history points are used to predict apatite fission track (AFT) ages and track length distributions.

4.5.1. Temperature Histories

[83] The T-t curves of Figure 10a depict the temperature evolution for the various history points through a steady temperature field. Temperature history curves from a stationary solution give temperature changes that are instant to the vertical motions of the HP through a fixed temperature field. On the other hand, the transient temperature component (Figure 10b) predicts the temperature perturbation from heat advection that is introduced by the displacement field.

[84] Perturbation from steady temperature conditions by heat advection can only occur by sufficiently vast effective vertical motions. The 1-D synthetic well modeling suggested that fast sedimentary loading renders temperature perturbations, whereas loading over a more extended period would maintain steady temperature conditions. The 2-D kinematic scenario builds from this, containing only 1–3 km Belly River overburden deposited over 25 Ma during initial upper Cretaceous contraction of the belt. Hence, at regional aver-

Figure 10. Temperature history curves for the selected history points in the kinematic model. (a) Steady state temperature evolution plotted along with the apatite partial annealing zone (PAZ). (b) Temperature perturbation (ΔT) from heat advection in the model. Temperature histories are plotted along with (c) organic maturation histories and (d) predictions on fission track length distributions from forward track length annealing modeling. For the forward modeling of fission track lengths, Durango AFT annealing kinetics are being adopted that are based on the regionally averaged findings of apatite composition [*Osadetz et al.*, 2004]. Furthermore, an annealing algorithm [*van der Beek*, 1995] has been used, based on methods explained by *Lutz and Omar* [1991] with a formation FT length of 15.8 μm.

age, such a scenario is least prone to temperature perturbation, unless introduced by smaller-scale fault block kinematics. The presented kinematic scenario is also conservative on the chance for perturbation from surface topography evolution by maintaining a smooth denudation profile. As a result, heat advection can occur by differential vertical motions of thrust sheets, most likely in structural culminations and strongly imbricated series where multiple thrust sheets achieve a stronger combined vertical displacement. The transient heat solution indeed predicts an advective temperature reduction for the HPs of 10–20°C relative to a stationary field between stages II and IV, a period with significant imbrication and stacking of sheets. However, the predicted temperature perturbation seems insufficient in amplitude and spatial coverage to result in a noticeable drop in paleotemperature gradients. Hence, our modeling, along with other studies [*Husson and Moretti*, 2002; *Deville and Sassi*, 2006; *Sassi et al.*, 2007], indicate that transient heat effects seem insignificant at first order in a thin-skinned thrust belt systems, even for complex kinematic scenarios.

[85] Despite the absence of significant temperature perturbations, modeled samples across the FFTB still record variable temperature histories (Figure 10a) depending on their stratigraphic and structural position. Till 70 Ma, the samples are heated mostly by sedimentary burial (stage I). For instance, HP3 is still close to surface with 25°C for the just deposited Belly River sediments, whereas HP2 gives 80°C being buried in Devonian strata to a depth of 3 km. At stage II, the temperature history (Figure 10a) controlled by sedimentary burial and loading and heat advection from thrust sheet emplacements. Furthermore, variable temperature evolutions occur for samples from the same stratigraphic interval as result of differential fault block motions (see HP1 and HP5 both located in the Cretaceous Blairmore Formation). Initially, HP1 is slightly deeper buried than HP5 from a westward increase in thickness of the foredeep sedimentary wedge. Afterward, the model predicts faster temperature increase and higher peak temperatures for HP5 as it gets buried under the triangle zone. For HP1 the temperature increase between stages II and IV is small as it is carried on top of a growing antiformal stack. Afterward, the temperature history of HP1 is unique in its recording of substantial post-Paleocene cooling (between stages V and VIII), as result of exhumation from out-of-sequence motions of the Livingstone thrust sheet by which it is carried. HP5 shows much slower cooling after stage IV, comparable to the other history points. The temperature histories of HPs 4 and 6 show much resemblance in the sedimentary burial they record, the first located in the roof thrust sheet of the triangle zone and the later at the base of the foreland basin sequence.

4.5.2. OMR History and AFT Predictions

[86] Predicted OMRs and AFT for the six HPs are respectively shown in Figures 10c and 10d. Maximum OMRs for all the HPs are reached only after time step IV. Hence, organic maturation occurs during the contraction of the belt and maximum values are reached after structures and potential traps for hydrocarbons have been formed.

[87] Predicted OMRs for the three HPs that reach surface (i.e., HPs 1, 4 and 6) are between 0.7 and 1.2%Ro, in the range of measured OMRs from surface samples in the foothills (Figure 3). HPs 2 and 5 never reached surface and experienced peak temperatures above 120°C and predict OMRs well above the regional average of 1.0–1.2% for the study area. The predictions of these two HPs correlate best with buried samples from Blairmore-Fernie and Paleozoic, respectively, strata from wells 07-27-6-3W5, 07-14-006-03W5, and 7-20-6-3W5 that show OMRs of 1.5%Ro and higher (Figure 4 and Table 1).

[88] The present-day fission track length distribution that are predicted for the different HPs, cover a wide range. Currently exposed synthetic samples (HPs 1, 4, and 6) yield high mean track lengths of 11–12 μm as they accumulated new fission tracks after moving out of the partial annealing zone (stage VI). On the other hand, still buried history points (HPs 2 and 5) have temperatures still in the partial annealing zone and consequently much shorter fission track distributions. Of the exhumed history points, HPs 4 and 6 give ages of ~50 Ma that reflect the contraction and first stage exhumation of the belt. Instead, HP1 records the out-of-sequence motion of the Livingstone thrust with an age of 34 Ma that coalesces with the large wavelength exhumation. Most of the available AFT data come from the Lewis thrust footwall, just east of its erosion front [*Osadetz et al.*, 2004]. Samples would also be needed for the more distal foothills portion to further test our modeling from AFT predictions and to better constrain especially the exhumation that presumably also involved the foreland.

5. Implications and Discussion

5.1. Similar OMRs From Variable Burial Histories

[89] Figure 11 gives a conceptual representation of our findings on the burial and temperature history of the FFTB. The chart displays a FFTB-like wedge that accommodates a maximum of 4–6 km burial. A steady state temperature gradient of ~25°C km^{-1} is also shown. Isotherms trend parallel relative to the developing topography as they are not distorted by motions in the thrust belt. Under steady state conditions, the temperatures that samples can reach are defined by the evolution of wedge bounding geometries, i.e., by the topography and basal decollement. The position of the basal decollement defines the maximum burial depth and temperatures that samples can hold in the system. For the situation shown in Figure 11, which is analog to our Canadian FFTB study area, samples can reach peak temperatures not higher than 100–150°C.

[90] The above example points us to the possibility that comparable ranks for samples from the same stratigraphic interval but different fault blocks do not require similar burial histories. It has been often assumed that comparable ranks between structures of different tectonic burial history, when coming from the same stratigraphic interval, point to similar sedimentary burial histories. Instead, comparable OMRs for the same stratigraphic interval across different structural entities can occur from different combinations of sedimentary and tectonic burial histories. This is clearly illustrated by the thermokinematic modeling where comparable peak burials and temperatures are reached for different stratigraphic

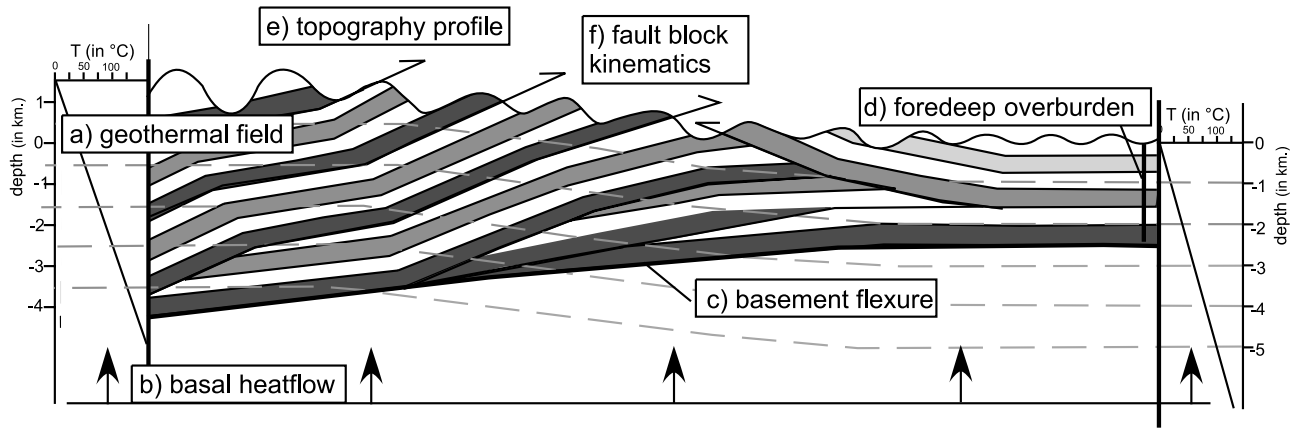

Figure 11. A schematic diagram highlighting the main factors in control of the burial and temperature and organic maturation history for a growing thrust belt system. The regional geothermal gradient (factor a) is defined by the basal heat flow (factor b) and thermal properties of the sediments in the belt. For the Canadian FFTB, a geothermal gradient of 20–25 mW m^{-2} is considered as a reasonable average. Down flexing of the basement (factor c) controls the burial history in the foreland basin (factor d). Furthermore, the basement flexure (factor c) also sets the position of the basal decollement of the growing wedge. Thickness of the wedge is controlled by the depth of the basement and the amount of topography (factor e). The isotherms within the evolving thrust belt at first-order trend parallel with the topography. Secondary distortions in the paleotemperature field might occur from fault block kinematics (factor f) and fluid flow (factor g). Yet, fault block kinematics (factor f) do affect the burial history and thereby the temperature history, even when the temperature field remains stationary. Recorded OMRs form an integration of these factors.

units from different combinations of sedimentary and tectonic loads (see Figure 10c; HP1 and HP3). Thus, samples actually acquire comparable ranks as they are constrained by the same wedge boundary conditions.

5.2. Temperature Perturbations

[91] The thermokinematic model of a thrust belt system not only predicts variable burial histories for samples with comparable OMRs, but also gives a range of OMR outcomes. Also when steady state temperature conditions prevail, variations in material pathways from the interplay of thrust sheet motions, basement flexure and surface erosion still produce a range of temperature histories. The cross-belt variations in OMRs can occur, by differential fault block motions and consequent differences in burial and temperature histories, also under steady state temperature conditions.

[92] Our explicit thermokinematic modeling examined if the displacement field of the belt (i.e., vertical motions from sedimentary burial and thrust sheet motions) render steady state or transient thermal conditions. Both fast sedimentary burial and vertical motions from thrust sheet displacement can produce perturbations in the temperature field. We showed from 1-D forward models how departures from steady state temperature conditions occur from fast predeformational sedimentary burial. When OMRs in the Fernie Basin would have formed by purely sedimentary burial, it requires fast burial of 5 km in short time span (less than 10 Ma) under perturbed temperature conditions. Instead, more time is available to reach peak burials by a combined sedimentary and tectonic burial history during the contraction of the belt. This would require a smaller initial sedimentary load of 3.5 km and steady state temperature conditions are being maintained.

[93] Subsequent 2-D thermokinematic modeling that contains a reduced initial sedimentary load produces only local-scale temperature perturbation. The growth of a duplex system can introduce some thermal perturbation when a combined displacement of multiple thrust sheets source locally elevated effective vertical motions. The kinematic history of the Turtle Mountain duplex system suggests some heat advection and perturbations of the temperature field. However, this example also sets clear limits to which perturbations can be expected. Heat advection in a thin-skinned thrust belt system is insufficient to introduce an overall drop in paleotemperature gradient.

[94] Previous studies have proposed a drop in paleotemperature gradient during contraction of the belt [*Osadetz et al.*, 2004]. These and our findings of low OMR values, despite large tectonic overburden [see also *Hardebol et al.*, 2007], suggest local temperature perturbations. The influence of fluid flow [e.g., *Forster and Smith*, 1989; *Bodri and Rybach*, 1998], or topographic and denudation [*Mancktelow and Grasemann*, 1997; *Stuwe and Hintermuller*, 2000] may need to be considered, where our paleotemperature constraints indicate perturbations while models show negligible effect of fault block motions.

5.3. Exhumation Phases

[95] In comparison to estimates of removed overburden from other studies, we argue for considering strongly reduced sedimentary loads for the SE Canadian FFTB. First, estimated overburdens include a stronger tectonic burial component

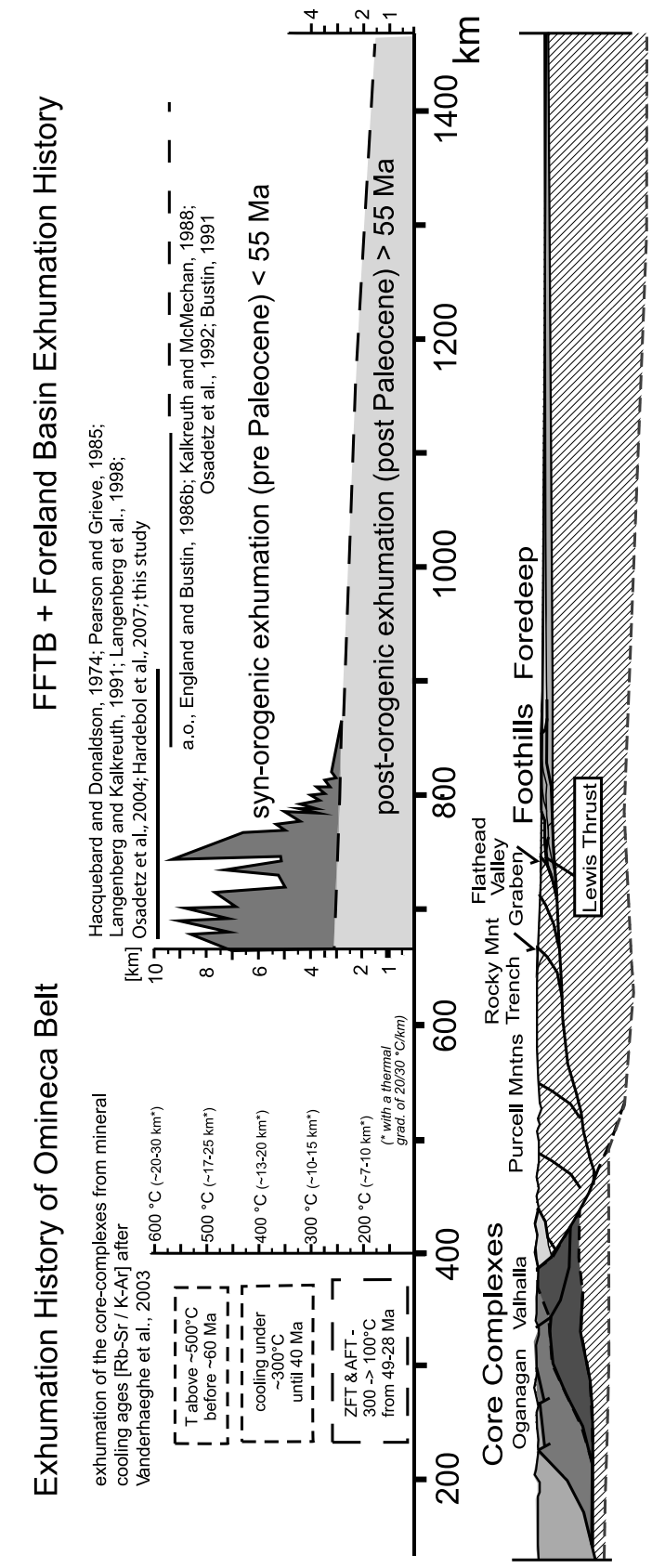

Figure 12. A schematic diagram outlining a multiphase exhumation history along an extended crustal-scale profile. For the FFTB, the erosion profile summarizes earlier restoration work [*Hardebol et al.*, 2007] combined with overburden estimation from OMRs and FT studies [this study; *Osadetz et al.*, 2004]. The large wavelength exhumation pattern is constrained by OMR studies in the basin [e.g., *Bustin*, 1991]. The exhumation history for the Intermontane Belt (the Oganagan, Valhalla, and Sushwap Core complexes) come from mineral cooling ages [e.g., *Parrish*, 1995; *Archibald et al.*, 1984; *Vanderhaeghe et al.*, 2003] and also record strong post-Paleocene exhumation.

than commonly assumed. Second, the paleotemperature gradient is not subdued to serious temperature drops from fault block motions during main contraction in the belt so that inversions of paleotemperature proxies to burial depths give moderate thicknesses.

[96] Examining the interplay between sedimentary and tectonic loads provides better understanding of the wavelengths and timing of overburden emplacement and removal. The forward kinematic modeling together with the restoration work [*Hardebol et al.*, 2007] highlight two episodes of exhumation for the FFTB (Figure 12). The short-wavelength exhumation of ~4–6 km for the first episode is estimated from the erosion profile in the restored cross section (Figure 7) and is associated with Late Cretaceous to early Paleocene thrusting. The forward kinematic scenario (Figure 9a) showed thrust sheets getting eroded at the exposed tips, but overall, the stacked sheets remained well preserved during the contraction of the belt.

[97] Only afterward, in post-Paleocene (mainly Eocene-Oligocene) times, the FFTB got further exhumed with 3–5 km erosion. This second episode involves large wavelength exhumation as it extends into the undeformed foreland with 3 km diminishing to 1 km, eastward over a distance of 1000 km. We consider that this postorogenic exhumation phase coincided with out-of-sequence displacement of the Livingstone thrust. Forward kinematic modeling showed how the Paleozoic in the Livingstone thrust sheet could only get emplaced atop of the Mesozoic foothills units after strong imbrication of the Mesozoic thrust sheets had occurred. At this point however, motion of the Livingstone thrust would have been hampered by the thick contracted wedge top that buried the Livingstone thrust sheet deeply. The overburden atop of the Livingstone thrust sheet requires removal to allow for more than 10 km motion of the sheet. As the Paleozoic strata in the Livingstone thrust sheet have overthrusted the Mesozoic thrust units, its emplacement most likely occurred along with substantial exhumation of the foothills.

[98] Last, displacement along the Livingstone thrust would imply a net eastward motion of the westerly located belts. The FFTB and particularly the Omineca Crystalline Belt to the west (Figure 1) record persuasive normal faulting in Eocene-Oligocene times (e.g., Flathead normal fault in FFTB and core complex formation to the west). The core complex formation is well documented [*Vanderhaeghe et al.*, 2003] and combines substantial normal faulting with postorogenic exhumation of the interior (Figure 12). The extensive normal faulting in Eocene-Oligocene times require a net eastward translation of the belts. Hence, out-of-sequence motion of the Livingstone thrust along with postorogenic exhumation of the FFTB fits well with core complex formation and exhumation in the Omineca Belt and with substantial denudation of the undeformed foreland in Eocene-Oligocene times.

6. Conclusions

[99] This study has analyzed the concurrent geothermal and kinematic evolution of the Canadian Cordilleran FFTB by assessing overburden histories from a newly compiled OMR catalog combined with forward modeling. Translation of OMR data into burial exhumation histories and overburden predictions require integration with conventional structural restoration work followed by forward burial and temperature history modeling. In this study, we have achieved this by combining a variety of structural controls with an extensive OMR data set and comparison with 2-D thermokinematic modeling.

[100] This study reveals significant regional variability in the OMR distribution for a representative portion of the SE Canadian FFTB (Figures 3 and 4). Combined sedimentary and tectonic burial components have been determined from individual wells or data clusters over specific structural entities. For instance, well 7-34-3-1W5 in the foothills gives a clear sedimentary burial trend with a correlation of OMRs to stratigraphic depth, whereas other adjacent wells around the Turtle mountain duplex record increasing OMRs for stratigraphic comparable but structural deeper levels. Thus, our OMR catalog in its entirety suppresses the idea of one exclusive mechanism (i.e., sedimentary versus tectonic burial) as coherent explanation for the observed OMR distribution.

[101] The 2-D kinematic modeling supports this conclusion by showing how inferred overburdens and peak temperatures can be reached by different combinations of sedimentary and tectonic burial from thrust sheet stacks. We show that a more moderate, than previously envisioned, sedimentary overburden of 3.5 km of Late Cretaceous sediments (Belly River Formation) is sufficient. Peak burials in the FFTB are subsequently reached with added load of thrust sheet stacks.

[102] Forward modeling also indicates that, apart from local perturbations in discrete structures, regional and steady paleogeothermal field with gradients in order of 20–25°C km^{-1} prevail, both during and after the Laramide orogeny. While the OMR distributions indicate some first-order correlation with combined sedimentary and tectonic burial, they also disclose local deviations from such regional trends. This might point to alternative controls on paleothermicity of thrust belt systems (e.g., perturbations entered by denudation history and fluid flow).

[103] This study shows how burial exhumation history predictions in structural complex areas like the Canadian FFTB are conditioned by a successful integration of conventional structural and restoration work with forward thermokinematic models that are constrained by thermochronological data. For the Canadian FFTB and adjacent foreland, such integration further reveals a short-wavelength synorogenic exhumation (~4–6 km) limited to the deformed foreland belt associated with thrust sheet emplacement during the Late Cretaceous–early Paleocene contraction, followed by a second episode of large wavelength exhumation involving the entire former foredeep (i.e., with amplitudes of 2 to 4 km) during the late Paleocene-Eocene.

[104] **Acknowledgments.** New OMR samples were made with the acknowledged aid of Daniel Pillot, who also assisted during the fieldwork. Well samples were provided by Devon Canada Inc., and the cooperation with Peter Fermor has been of great value for this work. Also thanked for constructive discussions are William Sassi and Marlies ter Voorde that helped to improve the modeling. Last, reviewers' comments have greatly helped further maturation of the paper.

References

Archibald, D. A., T. E. Krogh, R. L. Armstrong, and E. Farrar (1984), Geochronology and tectonic implications of magmatism and metamorphism, southern Kootenay Arc and neighbouring regions, southeastern British Columbia. Part II: Mid-Cretaceous to Eocene, *Can. J. Earth Sci.*, *21*, 567–583.

Bally, A. W., P. L. Gordy, and G. A. Stewart (1966), Structure, seismic data and orogenic evolution of southern Canadian Rocky Mountains, *Bull. Can. Pet. Geol.*, *14*, 337–381.

Barr, T. D., and F. A. Dahlen (1989), Brittle frictional mountain building: 2. Thermal structure and heat budget, *J. Geophys. Res.*, *94*, 3923–3947, doi:10.1029/JB094iB04p03923.

Batt, G. E., and M. T. Brandon (2002), Lateral thinking: 2-D interpretation of thermochronology in convergent orogenic settings, *Tectonophysics*, *349*, 185–201, doi:10.1016/S0040-1951(02)00053-7.

Beaumont, C. (1981), Foreland basins, *Geophys. J. R. Astron. Soc.*, *65*, 291–329.

Bodri, B., and L. Rybach (1998), Influence of topographically driven convection on heat flow in the Swiss Alps: A model study, *Tectonophysics*, *291*, 19–27, doi:10.1016/S0040-1951(98)00028-6.

Brewer, J. (1981), Thermal effects of thrust faulting, *Earth Planet. Sci. Lett.*, *56*, 233–244, doi:10.1016/0012-821X(81)90130-8.

Bustin, R. M. (1991), Organic maturity in the western Canada sedimentary basin, *Int. J. Coal Geol.*, *19*, 319–358, doi:10.1016/0166-5162(91)90026-F.

Carr, S. D. (1992), Tectonic Setting and U-Pb Geochronology of the early Tertiary Ladybird leucogranite suite, Thor-Odin-Pinnacles area, southern Omineca Belt, British Columbia, *Tectonics*, *11*, 258–278, doi:10.1029/91TC01644.

Constenius, K. N. (1996), Late Paleogene extensional collapse of the Cordilleran foreland fold and thrust belt, *Geol. Soc. Am. Bull.*, *108*, 20–39, doi:10.1130/0016-7606(1996)108<0020:LPECOT>2.3.CO;2.

Cooley, M. A., R. A. Price, J. M. Dixon, and T. K. Kyser (2006), Isotope geochemistry of fault zone samples from the Livingstone Range Anticlinorium and their significance to the thermal and fluid history of the southern Canadian foreland thrust and fold belt, *FRP Res. Rep. 12*, Queen's Univ., Kingston, Ont., Canada.

Currie, J. B., and S. O. Nwachukwu (1974), Evidence of incipient fracture porosity in reservoir rocks at depth, *Bull. Can. Pet. Geol.*, *22*, 42–58.

Dahlstrom, C. D. A. (1970), Structural geology in the eastern margin of the Canadian Rocky Mountains, *Bull. Can. Pet. Geol.*, *18*, 332–406.

Deville, E., and W. Sassi (2006), Contrasting thermal evolution of thrust systems: An analytical and modeling approach in the front of the western Alps, *AAPG Bull.*, *90*, 887–907, doi:10.1306/01090605046.

Durand, B., B. Alpern, J. L. Pittion, and B. Pradier (1986), Thermal modeling in sedimentary basins, in *Thermal Modeling in Sedimentary Basins*, edited by J. Burrus, pp. 441–475, Technip, Paris.

Ehlers, T. A., and K. A. Farley (2003), Apatite (U-Th)/He thermochronometry: Methods and applications to problems in tectonic and surface processes, *Earth Planet. Sci. Lett.*, *206*, 1–14, doi:10.1016/S0012-821X(02)01069-5.

Endignoux, L., and S. Wolf (1990), Thermal and kinematic evolution of thrust basins: A 2D numerical view, in *Petroleum and Tectonics in Mobile Belts*, edited by J. Letouzey, pp. 181–192, Technip, Paris.

England, P. C., and A. B. Thompson (1984), Pressure-temperature-time paths of regional metamorphism I. Heat transfer during the evolution of regions of thickened continental crust, *J. Petrol.*, *25*, 894–928.

England, T. D. J., and R. M. Bustin (1986a), Effect of thrust faulting on organic maturation in the southeastern Canadian Cordillera, *Adv. Org. Geochem.*, *10*, 609–616, doi:10.1016/0146-6380(86)90057-4.

England, T. D. J., and R. M. Bustin (1986b), Thermal maturation of the western Canadian sedimentary basin south of the Red Deer River: I. Alberta Plains, *Bull. Can. Pet. Geol.*, *34*, 71–90.

Espitalié, J. (1986), Use of Tmax as a maturation index for different types of organic matter: Comparison with vitrinite reflectance, in *Thermal Modeling in Sedimentary Basins*, edited by J. Burrus, pp. 475–496, Technip, Paris.

Faure, J. L., K. Osadetz, N. Benaouali, F. Schneider, and F. Roure (2004), Kinematic and petroleum modeling of the Alberta Foothills and adjacent foreland, west of Calgary, *Rev. Inst. Fr. Pet.*, *59*, 81–108.

Fermor, P. R., and I. W. Moffat (1992), Tectonics and structure of the Western Canada Foreland Basin, in *Foreland Basins and Fold Belts*, edited by R. W. Macqueen and D. A. Leckie, *AAPG Mem.*, *55*, 81–105.

Forster, C., and L. Smith (1989), The influence of groundwater flow on thermal regimes in mountainous terrain: A model study, *J. Geophys. Res.*, *94*, 9439–9451, doi:10.1029/JB094iB07p09439.

Gabrielse, H., and C. J. Yorath (1992), *The Geology of Canada*, vol. 4, *Geology of the Cordilleran Orogen in Canada*, 847 pp., Geol. Surv. of Can., Ottawa.

Hacquebard, P. A. (1977), Rank of coal as an index of organic metamorphism for oil and gas in Alberta, *Geol. Surv. Can. Bull.*, *262*, 11–22.

Hacquebard, P. A., and J. R. Donaldson (1974), Rank studies of coals in the Rocky Mountains and Inner Foothills Belt Canada, *Spec. Pap. Geol. Soc. Am.*, *153*, 75–94.

Hannigan, P., P. J. Lee, K. G. Osadetz, and K. Olsen-Heise (1993), Oil and gas resource potential of the Kooteney area of British Columbia, internal report prepared for British Columbia Energy and Petroleum Resources, Geol. Surv. of Can., Calgary, Alberta.

Hardebol, N. J., J. P. Callot, J. L. Faure, G. Bertotti, and F. Roure (2007), Kinematics of the SE Canadian Fold and Thrust Belt: Implications for the thermal and organic maturation history, in *Thrust Belts and Foreland Basins: From Kinematics to Hydrocarbon Systems*, edited by O. Lacombe et al., pp. 179–202, doi:10.1007/978-3-540-69426-7_10, Springer, Berlin.

Hitchon, B. (1984), Geothermal gradients, hydrodynamics and hydrocarbon occurrences, Alberta, Canada, *AAPG Bull.*, *68*, 713–743.

Hughes, J. T. R. (1987), *The Finite Element Method: Linear Static and Dynamic Finite Element Analysis*, Prentice-Hall, Englewood Cliffs, N. J.

Husson, L., and I. Moretti (2002), Thermal regime of fold and thrust belts–an application to the Bolivian sub-Andean zone, *Tectonophysics*, *345*, 253–280, doi:10.1016/S0040-1951(01)00216-5.

Kalkreuth, W., and C. W. Langenberg (1986), The timing of coalification in relation to structural events in the Grande Cache area, Alberta, *Can. J. Earth Sci.*, *23*, 1103–1116, doi:10.1139/e86-110.

Kalkreuth, W., and M. McMechan (1988), Burial history and thermal maturity, Rocky Mountain Front ranges, foothills, and foreland, east-central British Columbia and adjacent Alberta, Canada, *AAPG Bull.*, *72*, 1395–1410.

Kalkreuth, W., W. Langenberg, and M. McMechan (1989), Regional coalification pattern of Lower Cretaceous coal-bearing strata, Rocky Mountain Foothills and foreland, Canada—Implications for future exploration, *Int. J. Coal Geol.*, *13*, 261–302, doi:10.1016/0166-5162(89)90096-7.

Labrecque, J. E., and E. W. Shaw (1973), Restoration of Basin and Range faulting across the Howell Creek Window and Flathead valley of southeastern British Columbia, *Bull. Can. Pet. Geol.*, *21*, 117–122.

Lampe, C., and M. Person (2002), Advective cooling within sedimentary rift basins—Application to the Rhinegraben (Germany), *Mar. Pet. Geol.*, *19*, 361–375, doi:10.1016/S0264-8172(02)00022-3.

Lampe, C., M. Person, S. Noth, and W. Ricken (2001), Episodic fluid flow within continental rift basins: Some insights from field data and mathematical models of the Rhinegraben, *Geofluids*, *1*, 42–52, doi:10.1046/j.1468-8123.2001.11005.x.

Langenberg, C. W., W. Kalkreuth, and K. Holmes (1998), Components of syn- and post-deformational coalification in the Mountain Park area west central Alberta, *Bull. Can. Pet. Geol.*, *46*, 564–575.

Langenberg, C. W., A. Beaton, and H. Berhane (2002), Regional evaluation of the coalbed methane potential of the foothills/mountains of Alberta, *EUB/AGS Earth. Sci. Rep. 2002-05*, Alberta Geol. Surv., Edmonton, Canada.

Langenberg, W., and W. Kalkreuth (1991), Tectonic controls on regional coalification and vitrinite-reflectance anisotropy of Lower Cretaceous coals in the Alberta Foothills, Canada, *Bull. Soc. Geol. Fr.*, *162*, 375–383.

Lock, J., and S. Willett (2008), Low temperature thermochronometric ages in fold-and-thrust belts, *Tectonophysics*, *456*, 147–163, doi:10.1016/j.tecto.2008.03.007.

Lutz, T. M., and G. Omar (1991), An inverse method of modeling thermal histories from apatite fission-track dates, *Earth Planet. Sci. Lett.*, *104*, 181–195, doi:10.1016/0012-821X(91)90203-T.

Magara, K. (1976), Thickness of removed sedimentary rocks, paleopore pressure and paleotemperature, southwestern part of western Canada Basin, *AAPG Bull.*, *60*, 554–565.

Mancktelow, N. S., and B. Grasemann (1997), Time-dependent effects of heat advection and topography on cooling histories during erosion, *Tectonophysics*, *270*, 167–195, doi:10.1016/S0040-1951(96)00279-X.

McMechan, M. E., and R. A. Price (1982), Superimposed low-grade metamorphism in the Mount Fisher area, southeastern British Columbia—Implications for the East Kootenay orogeny, *Can. J. Earth Sci.*, *19*, 476–489, doi:10.1139/e82-039.

McMechan, R. D., and R. A. Price (1980), Reappraisal of a reported unconformity in the Paleogene (Oligocene) Kishenehn Formation: Implications for Cenozoic tectonics in the Flathead Valley graben, southeastern British Columbia, *Bull. Can. Pet. Geol.*, *28*, 37–45.

Middleton, M. F. (1982), Tectonic history from vitrinite reflectance, *Geophys. J. R. Astron. Soc.*, *68*, 121–132.

Moore, M. A., and P. C. England (2001), On the inference of denudation rates from cooling ages of minerals, *Earth Planet. Sci. Lett.*, *185*, 265–284, doi:10.1016/S0012-821X(00)00380-0.

Osadetz, K. G., F. W. Jones, J. A. Majorowicz, D. E. Pearson, and L. D. Stasiuk (1992), Thermal history of the Cordilleran Foreland Basin in western Canada: A review, in *Foreland Basins and Fold Belts*, edited by R. W. Macqueen and D. A. Leckie, *AAPG Mem.*, *55*, 259–278.

Osadetz, K., B. Kohn, S. Feinstein, and R. Price (2004), Deformation, fluid flow and reservoir appraisal, in Foreland fold and thrust belts, in *Deformation, Fluid Flow, and Reservoir Appraisal in Foreland Fold and Thrust Belts, AAPG Hedberg Ser.*, vol. 1, edited by R. Swennen, F. Roure, and J. W. Granath, pp. 21–48, Am. Assoc. of Pet. Geol., Tulsa, Okla.

Parrish, R. R. (1995), Thermal evolution of the southeastern Canadian Cordillera, *Can. J. Earth Sci.*, *32*, 1618–1642.

Pearson, D. E., and D. A. Grieve (1985), Rank variation, coalification pattern and coal quality in the Crowsnest coalfield, British Columbia, *Can. Inst. Min. Metall. Bull.*, *78*(881), 39–46.

Peper, T. (1993), Tectonic control on the sedimentary record in foreland basins: Inferences from quantitative subsidence analyses and stratigraphic modeling, Ph.D. thesis and supplement, Vrije Univ., Amsterdam.

Peters, K. E. (1986), Guidelines for evaluating petroleum source rock using programmed pyrolysis, *AAPG Bull.*, *70*, 318–329.

Price, R. A. (1981), The Cordilleran foreland thrust and fold belt in the southern Canadian Rocky Mountains, in *Thrust and Nappe Tectonics*, edited by K. R. McClay and N. V. Price, *Geol. Soc. Spec. Publ.*, *9*, 426–448.

Price, R. A. (2001), An evaluation of models for the kinematic evolution of thrust and fold belts: Structural analysis of a transverse fault zone in the Front Ranges of the Canadian Rockies north of Banff, Alberta, *J. Struct. Geol.*, *23*, 1079–1088, doi:10.1016/S0191-8141(00)00177-2.

Price, R. A., and P. R. Fermor (1985), Structure section of the Cordilleran foreland thrust and fold belt west of Calgary, Alberta, *Pap. Geol. Surv. Can.*, *84-14*.

Price, R. A., and P. R. Fermor (1994), Structure section of the Cordilleran foreland thrust and fold belt west of Calgary, Alberta, 1:50000 and 1:250000 sections and 1:250000 palinspastically restored section, *Pap. Geol. Surv. Can.*, *84-14*, 1 sheet.

Price, R. A., and J. W. Sears (2000), A preliminary palinspastic map of the Mesoproterozoic Belt-Purcell Supergroup, Canada and USA: Implications for the tectonic setting and structural evolution of the Purcell anticlinorium and the Sullivan deposit, in *The Geological Environment of the Sullivan Deposit, British Columbia*, *Spec. Publ.*, vol. 1, edited by J. W. Lydon et al., pp. 61–81, Miner. Deposits Div., Geol. Assoc. of Can., LOCATION.

Roure, F., and W. Sassi (1995), Kinematic of deformation and petroleum system appraisal in Neogene foreland-fold-and-thrust belts, *Petrol. Geosci.*, *1*, 253–269.

Roure, F., R. Swennen, F. Schneider, J. L. Faure, H. Ferket, N. Guilhaumou, K. Osadetz, P. Robion, and V. Vandeginste (2005), Incidence and importance of tectonics and natural fluid migration on reservoir evolution in foreland fold-and-thrust belts, *Oil Gas Sci. Technol.*, *60*, 67–106.

Ruppel, C., and K. V. Hodges (1994), Pressure-temperature-time paths from two-dimensional thermal models: Prograde,retrograde and inverted metamorphism, *Tectonics*, *13*, 17–44, doi:10.1029/93TC01824.

Sassi, W., and J. L. Rudkiewicz (1999), THRUSTPACK version 6.2: 2D integrated maturity studies in thrust areas, *IFP Rep. 45372*, 79 pp., Inst. Fr. du Pét., Rueil-Malmaison, France.

Sassi, W., R. Graham, R. Gillcrist, M. Adams, and R. Gomez (2007), The impact of deformation timing on the prospectivity of the Middle Magdalena subthrust, Colombia, in *Deformation of the Continental Crust: The Legacy of Mike Coward*, edited by A. C. Ries, R. W. H. Butler, and R. H. Graham, *Geol. Soc. Spec. Publ.*, *272*, 473–498.

Sears, J. W. (2001), Emplacement and denudation history of the Lewis-Eldorado-Hoadley thrust slab in the northern Montana Cordillera, USA: Implications for steady-state orogenic processes, *Am. J. Sci.*, *301*, 359–373, doi:10.2475/ajs.301.4-5.359.

Snowdon, L. R. (1997), Rock-Eval/TOC data for six Alberta foothills wells (townships 23 to 27 and ranges 5W5 to 7W5, *Geol. Surv. Can. Open File*, *3493*.

Stasiuk, L. D., and M. G. Fowler (2002), Thermal maturity evaluation (vitrinite and vitrinite reflectance equivalent) of Middle Devonian, Upper Devonian, and Mississippian strata in the western Canada Sedimentary Basin [CD–ROM], *Geol. Surv. Can. Open File*, *4341*.

Stasiuk, L. D., M. G. Fowler, and G. Addison (2002), Thermal maturity evaluation of Lower Cretaceous Mannville Group and equivalent coals in the western Canada Sedimentary Basin: A compilation of vitrinite reflectance data, *Geol. Surv. Can. Open File*, *4342*.

Stuwe, K., and M. Hintermuller (2000), Topography and isotherms revisited: The influence of laterally migrating drainage divides, *Earth Planet. Sci. Lett.*, *184*, 287–303, doi:10.1016/S0012-821X(00)00315-0.

Sweeney, J. J., and A. K. Burnham (1990), Applications of a simple model of vitrinite reflectance based on chemical kinetics, *AAPG Bull.*, *74*, 1559–1570.

Teichmüller, M. (1986), Organic petrology of source rocks, history and state of the art, *Adv. Org. Geochem.*, *10*, 581–599, doi:10.1016/0146-6380(86)90055-0.

ter Voorde, M., C. H. de Bruijne, S. A. P. L. Cloetingh, and P. A. M. Andriessen (2004), Thermal consequences of thrust faulting: Simultaneous versus successive fault activation and exhumation, *Earth Planet. Sci. Lett.*, *223*, 395–413, doi:10.1016/j.epsl.2004.04.026.

Tissot, B. (2003), Preliminary data on the mechanisms and kinetics of the formation of petroleum in sediments: Computer simulation of a reaction flowsheet, *Oil Gas Sci. Technol.*, *58*, 183–202.

Tissot, B., R. P. Pelet, and P. Ungerer (1987), Thermal history of sedimentary basins, maturation indices, and kinetics of oil and gas generation, *AAPG Bull.*, *71*, 1445–1466.

Ungerer, P., J. Burrus, B. Doligez, P. Y. Chnet, and F. Bessis (1990), Basin evaluation by integrated two-dimensional modeling of heat transfer, fluid flow, hydrocarbon generation and migration, *AAPG Bull.*, *74*, 309–335.

van der Beek, P. A. (1995), Tectonic evolution of continental rifts: Inferences from numerical modelling and fission track thermochronology, Ph.D. thesis, 232 pp., Vrije Univ., Amsterdam.

van der Pluijm, B. A., P. J. Vrolijk, D. R. Pevear, C. M. Hall, and J. Solum (2006), Fault dating in the Canadian Rocky Mountains: Evidence for late Cretaceous and early Eocene orogenic pulses, *Geology*, *34*, 837–840, doi:10.1130/G22610.1.

Vanderhaeghe, O., C. Teyssier, I. McDougall, and W. J. Dunlap (2003), Cooling and exhumation of the Suswap Metamorphic Core Complex constrained by $^{40}Ar/^{39}Ar$ thermochronology, *Geol. Soc. Am. Bull.*, *115*, 200–216, doi:10.1130/0016-7606(2003)115<0200:CAEOTS>2.0.CO;2.

G. Bertotti and N. J. Hardebol, Netherlands Research Centre for Integrated Solid Earth Sciences, Faculty of Earth and Life Science, Vrije Universiteit, De Boelelaan 1085, NL-1081 HV Amsterdam, Netherlands. (nico.hardebol@falw.vu.nl)

J. P. Callot and J. L. Faure, Institut Français du Pétrole, 1-4 avenue de Bois Préau, F-92852 Rueil Malmaison CEDEX, France.